



Norwegian University of
Science and Technology

Studies of Combustion in Berkeley's Vitiated Co-flow burner

Birgitte Johannessen

Master of Science in Energy and Environment

Submission date: June 2011

Supervisor: Terese Løvås, EPT

Co-supervisor: Robert Dibble, University of California at Berkeley

EPT-M-2011-16

MASTER THESIS

for

Birgitte Johannessen

Stud.techn.
Spring 2011*Studies of Combustion in Berkeley's Vitiated Co-flow Burner (VCB)**Studier av Forbrenning i Berkeleys medstroms brenner (VCB)***Background and objective.**

In order to meet requirements for clean energy, CO₂ capture technologies are under development such as combustors for hydrogen or hydrogen enriched fuels. The main challenge regarding burning such fuels are the high burning temperatures and the modified flammability limits and stability ranges compared to conventional fuels. This requires in turn modification of the combustors. However, it is of course desirable to minimise these modifications from an economical and safety point of view. Hence, much research is devoted to understand and control hydrogen combustion in conventional like combustors, both through numerical studies and experimental work. The Master thesis of Birgitte Johannessen will be linked to already existing research in this area devoted to study hydrogen combustion at elevated pressures. The work will involve becoming familiar with experimental research and developing an experimental set-up for the vitiated co-flow burner at Berkeley University, California, US. This work is directly related to her Project thesis which involved numerical simulations of flame propagation in channel flows. This is furthermore part of a large international research project, BIGCCS, on carbon capture technologies, including NTNU and Sintef Energy.

The following questions should be considered in the project work:

Birgitte Johannessen will be part of the world leading research group at Berkeley University lead by Prof. Robert Dibble. This will mean getting experience with state-of-the-art experimental research on combustion and modern measurement techniques.

Birgitte will lead an experimental investigation in characterizing the frequency of ignition and extinction of unsteady flames produced with Berkeley's Vitiated Co-flow Burner (VCB). The VCB consists of a co-flow generated from lean premixed hydrogen combustion that surrounds a central jet consisting of a mixture of hydrogen and nitrogen. The primary purpose of the VCB is to investigate the effects of co-flow temperature (co-flow equivalence ratio), jet velocity, and nitrogen dilution on the liftoff height of lifted flames. It has been observed, however, that with elevated co-flow equivalence ratios and nitrogen dilution mole fractions, lifted flames can no longer be generated. Instead, the flame is characterized by rapid ignition followed by a gradual blow-off event. It is therefore prudent to gain a better understanding of the

nature of these unsteady flames. This characterization is the subject of Birgitte's research focus while in Berkeley.

The primary output of this research is the determination of a relationship between the frequency of blow-off and re-ignition as a function of co-flow equivalence ratio, jet velocity, and nitrogen dilution mole fraction. This frequency will be measured in a number of ways. First, a high resolution microphone will be used to investigate the time-amplitude response of the noise emitted from the flame. It has been observed that the re-ignition event is characterized by a high amplitude acoustic wave emitted from the flame, so this can be used as a marker for determining the time of re-ignition. An average frequency of ignition and blow-off can then be determined through post processing of the data.

In the effort to be able to process the sound profiles emanating from a range of flames in a consistent manner, Birgitte will develop post processing techniques to convert the time-sound data to a more useful format. Using the data gathered from the sound files of various flames, Birgitte will summarize the trends of the frequencies of ignition and extinction and draw conclusions based on these results.

Under some circumstances, it can be difficult to discern whether a peak in the time-amplitude acoustic response from the flame is indicative of an ignition event. Consequently, it is necessary to guide the analysis of this data using an independent means of examining these flames. High speed schlieren imaging will be used for this purpose. Birgitte will examine the high speed schlieren videos of the unsteady flames that she generates. This data will be compared to the sound data as a means of calibrating her post processing techniques and will serve as a means of validating this data.

Birgitte will carry out this development together with graduate student Andrew North directly supervised by Prof. Dibble.

-- " --

Within 14 days of receiving the written text on the master thesis, the candidate shall submit a research plan for his project to the department.

When the thesis is evaluated, emphasis is put on processing of the results, and that they are presented in tabular and/or graphic form in a clear manner, and that they are analyzed carefully.

The thesis should be formulated as a research report with summary both in English and Norwegian, conclusion, literature references, table of contents etc. During the preparation of the text, the candidate should make an effort to produce a well-structured and easily readable report. In order to ease the evaluation of the thesis, it is important that the cross-references are correct. In the making of the report, strong emphasis should be placed on both a thorough discussion of the results and an orderly presentation.

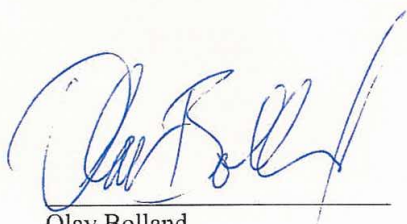
The candidate is requested to initiate and keep close contact with his/her academic supervisor(s) throughout the working period. The candidate must follow the rules and regulations of NTNU as well as passive directions given by the Department of Energy and Process Engineering.

Pursuant to "Regulations concerning the supplementary provisions to the technology study program/Master of Science" at NTNU §20, the Department reserves the permission to utilize all the results and data for teaching and research purposes as well as in future publications.

One – 1 complete original of the thesis shall be submitted to the authority that handed out the set subject. (A short summary including the author's name and the title of the thesis should also be submitted, for use as reference in journals (max. 1 page with double spacing)).

Two – 2 – copies of the thesis shall be submitted to the Department. Upon request, additional copies shall be submitted directly to research advisors/companies. A CD-ROM (Word format or corresponding) containing the thesis, and including the short summary, must also be submitted to the Department of Energy and Process Engineering

Department of Energy and Process Engineering, 17. January 2011



Olav Bolland
Department Head



Terese Løvås
Academic Supervisor

Research Advisors:

Andrea Gruber, Sintef Energy, Trondheim, Norway
Robert Dibble, Berkeley University, California, US.

Preface

This report *Studies of Combustion in Berkeley's Vitiated Co-flow Burner* is the result of undersigned's Master Thesis at the Norwegian University of Science and Technology (NTNU), in the spring semester of 2011. The work was carried out at the Department of Mechanical Engineering at University of California Berkeley. This master thesis is a part of the BIGCCS research project.

The objective of the thesis was to investigate unsteady hydrogen jet-flames diluted with nitrogen issued into a vitiated co-flow consisting of products of lean premixed combustion of hydrogen with air. The N_2 - H_2 jet flame was studied experimentally with the emphasis on the ignition frequency of the unsteady flame. The flame was investigated by the use of audio recordings and Schlieren imaging high speed video. The purpose of the research was to determine a relationship of the frequency of blowout and re-ignition as a function of co-flow temperature, jet velocity and nitrogen dilution mole fraction.

I would like express my gratitude to PhD candidate Andrew North. His help, support and guidance is strongly appreciated. Thanks to my advisors Professor Terese Løvås at NTNU and Professor Robert Dibble at UC Berkeley. I would also like to thank Jan Olav Owren for his help with the signal analysis and John Henry for proofreading. A special thanks goes to Bjarne Betjent for teaching me how to count.



Birgitte Johannessen
Berkeley, June 2011

Abstract

An experimental investigation is presented of unsteady N_2 - H_2 jet flames in a co-flow of hot combustion products of lean premixed hydrogen combustion. The unsteady jet flame is characterized by rapid ignition followed by a gradually blowout of the flame. Audio recordings and Schlieren imaging high speed videos are used to investigate the unsteady flame. The frequency of the blowout-re-ignition event is investigated as a function of nitrogen dilution mole fraction ($Y_{N_2}=0.180-0.566$), co-flow equivalence ratio ($\Phi_{co-flow}=0.20-0.27$) and jet velocity ($V_{jet}=300-500$ m/s). The results from the audio recordings and Schlieren imaging high speed videos indicate that re-ignition of the flame occurs as a result of autoignition. The ignition frequency increases with increasing nitrogen dilution mole fraction until a maximum frequency is reached of about 20-27 Hz. After the maximum frequency is reached the frequency decreases with a further increase of the nitrogen dilution mole fraction until the flame is completely blown out. By increasing the co-flow equivalence ratio the flame becomes unsteady and blown out at increasing nitrogen dilution mole fractions. The range of nitrogen dilution mole fractions over which the flame is unsteady is decreasing with increasing co-flow equivalence ratio. By increasing the jet velocity the flame with low co-flow equivalence ratios ($\Phi_{co-flow}=0.20-0.22$) becomes unsteady and blown out for decreasing nitrogen dilution mole fractions. For higher co-flow equivalence ratios ($\Phi_{co-flow}=0.24-0.27$) the range of nitrogen dilution mole fractions over which the flame is unsteady increases with increasing velocity. An increase in the velocity at higher co-flow equivalence ratios leads to an unsteady flame for lower nitrogen dilution mole fractions and a blown out flame for higher nitrogen dilution mole fractions. These results suggests that the autoignition phenomena of the N_2 - H_2 jet flame issued into a vitiated co-flow is controlled by both chemistry and turbulent mixing. The results from the audio recordings and the Schlieren imaging high speed videos correspond well. This gives confidence to using audio recordings as a method of diagnostics of unsteady hydrogen jet flames.

Sammendrag

En eksperimentell studie av ustabile N_2 - H_2 jetflammer i en medstrøm generert av forbrenning av mager forblandet hydrogen blir presentert. Den ustabile jetflammen er karakterisert av hurtig antenning fulgt av gradvis utblåsing av flammen. Lydopptak og Schlieren fotografering høyhastighetsvideo blir brukt til å studere den ustabile flammen. Frekvensen av utblåsing - antenning av flammen blir studert som funksjon av nitrogenutblandingsmolfraksjon ($Y_{N_2}=0.180-0.566$), medstrømsblandingsforhold ($\Phi_{co-flow} = 0.20-0.27$) og jethastighet ($V_{jet}=300-500$ m/s). Resultatene fra lydopptakene og høyhastighetsvideoene antyder at antenningen av flammene skjer som resultat av selvantenning. Antenningsfrekvensen øker med økende molfraksjon av nitrogenutblending opp til et punkt der maksimum frekvens er nådd ved en frekvens på rundt 20-27 Hz. Etter maksimum frekvens er nådd synker frekvensen ved videre øking av molfraksjonen av nitrogenutblending inntil flammen blåses ut. Ved å øke blandingsforholdet til medstrømmen blir flammen ustabil og blåses ut ved økende nitrogenutblandingsmolfraksjon. Området av nitrogenutblandingsmolfraksjoner der flammen er ustabil minker med økende medstrøms blandingsforhold. Ved å øke jethastigheten blir flammen ustabil og blåses ut ved minkende molfraksjon av nitrogenutblending for lave blandingsforhold av medstrømmen ($\Phi_{co-flow}=0.20-0.22$). For høyere blandingsforhold av medstrømmen ($\Phi_{co-flow}=0.24-0.27$) øker området over nitrogenutblandingsmolfraksjoner der flammen er ustabil med økende jethastighet. Disse resultatene antyder at selvantenningsfenomenet til N_2 - H_2 jetflammen i en varm medstrøm er kontrollert av både kjemi og turbulent blanding. Resultatene fra lydinnspillingene og høyhastighet kameraopptakene viser godt samsvar med hverandre. Dette gir tillit til at lydopptak kan brukes som diagnostikk for studier av ustabile hydrogenjetflammer.

Nomenclature

Latin letters

D	Diffusion coefficient	[m ² /s]
<i>f</i>	Frequency	[Hz]
<i>i</i>	Imaginary unit	-
L	Length	[m]
M	Filter width for moving average filter	-
<i>m_a</i>	Mass of air	[kg]
<i>m_f</i>	Mass of fuel	[kg]
n	number of measurements	-
<i>P_{\bar{x}}</i>	Random uncertainty of the mean of x	-
R	Result	Various units
Re	Reynolds number	-
<i>S_l</i>	Laminar flame speed	[m/s]
<i>S_x</i>	Standard deviation	Various units
T	Temperature	[K]
t	Student's t coefficient	-
u	velocity	[m/s]
u'	Fluctuation of velocity	[m/s]
$\langle V \rangle$	Mean velocity	[m/s]
<i>W_{\bar{x}}</i>	Total uncertainty of the mean of x	-
<i>x[i]</i>	Input signal	Various units
<i>Y_i</i>	Mole fraction of species <i>i</i>	-
<i>y[i]</i>	Output signal	Various units
<i>Z_i</i>	Elemental mass fraction of element <i>i</i>	-

Greek symbols

μ	Dynamic viscosity	[kg/ms]
ν	Kinematic viscosity	[m ² /s]
ξ	Mixture fraction	-
ρ	Density	[kg/m ³]
τ	Shear stress	[Pa]
Φ	Equivalence ratio	-
χ	Scalar dissipation rate	[1/s]
ω_R	Systematic uncertainty in a result	-
ω_{x_i}	Systematic uncertainty in the variable x_i	-

Contents

Preface	i
Abstract	iii
Sammendrag	v
Nomenclature	vii
1. Introduction	1
2. Theory	5
2.1. Turbulence	5
2.2. Combustion	8
2.2.1. Premixed Combustion	8
2.2.2. Non-Premixed Combustion	9
2.2.3. Flame Stabilization	12
2.3. Gas Turbine Combustion and NO_x Control	13
2.4. Hydrogen Fundamentals	17
2.5. Measurement Uncertainty	20
2.5.1. Random Uncertainties	20
2.5.2. Systematic Uncertainties	21
2.5.3. Estimate of Total Uncertainty	21
2.6. Signal Processing	23
2.6.1. Filters	24
3. Prior Work	25
4. Experimental Objective	31
5. Experimental Apparatus	33
5.1. Berkeley's Vitiated Co-flow Burner	33
5.2. Schlieren Imaging System	37
5.3. Microphone Diagnostic	41

6. Methodology	43
6.1. Audio Signal Analysis	45
6.2. Video Analysis	51
7. Results and Discussion	53
7.1. Comparison with Previous Experiment	53
7.2. Characterization of the Unsteady Flame	55
7.3. Frequency of the Ignition Event	57
7.3.1. Results from the Audio Signal Analysis	59
7.3.2. Results from the Video Analysis	68
7.4. Comparison between Audio and Video Results	70
7.5. Uncertainty Analysis	73
7.5.1. Uncertainty of the Audio Recordings	73
7.5.2. Uncertainty Analysis of the High Speed Video	77
8. Conclusion	79
9. Suggestions for further work	81
A. Table of results from the experiments	87
A.1. Results from Audio Recordings	87
A.2. Results from High Speed Videos	93
B. Calculation of the systematic uncertainty	97
C. Calculation of random uncertainty	101
D. MATLAB scripts	103
D.1. Count peaks script	103
D.2. FFT script	104
D.3. Integral method	105
D.4. Background correction	106

List of Figures

1.1.	Gasification of fossil fuels.	3
2.1.	Turbulent velocity signal.	6
2.2.	Lifted jet flame.	11
2.3.	Schematics of a gas turbine with a non-premixed combustor design.	14
2.4.	Schematics of a two staged gas turbine with a premixed combustor design.	14
2.5.	Laminar flame speed of N ₂ -H ₂ flames.	18
3.1.	Liftoff heights normalized by the Reynolds number.	28
3.2.	Stability diagrams for N ₂ -H ₂ flames.	30
5.1.	Schematics of the Vitiated Co-flow Burner [North, 2010].	34
5.2.	The vitiated Co-flow Burner at Berkeley.	36
5.3.	Conceptual drawing of the schlieren imaging system.	37
5.4.	Direct imaging of hydrogen jet flame.	38
5.5.	Comparison of liftoff heights clearly made visible by the schlieren imaging system.	39
5.6.	Schlieren Imaging System used in the experiments.	40
5.7.	The experimental apparatus of the Vitiated Co-flow Burner with the Schlieren imaging system and microphone.	42
6.1.	Raw unfiltered time-amplitude response for jet flame with $V_{jet}=400$ m/s, $\Phi_{co-flow}=0.20$ and $Y_{N_2}=0.324$	46
6.2.	Filtered time-amplitude response for jet flame with $V_{jet}=400$ m/s, $\Phi_{co-flow}=0.20$ and $Y_{N_2}=0.324$ with three different filter widths.	47
6.3.	Frequency response of sound recordings of jet flame with $V_{jet}=400$ m/s $\Phi_{co-flow}=0.20$ and $Y_{N_2}=0.407$	48
6.4.	Filtered time-amplitude response of jet flame with $V_{jet}=400$ m/s, $\Phi_{co-flow}=0.20$ and $Y_{N_2}=0.407$	49

List of Figures

7.1. Stability diagrams.	54
7.2. Schlieren image of lifted N ₂ -H ₂ jet flame in a vitiated co-flow.	55
7.3. Schlieren images of ignition event.	56
7.4. Audio signal of one ignition event for N ₂ -H ₂ jet flame with V _{jet} =300 m/s, Φ _{co-flow} =0.20 and Y _{N₂} =0.432.	56
7.5. Audio signal for N ₂ -H ₂ jet flame with V _{jet} =500 m/s, Y _{N₂} =0.229 and Φ _{co-flow} =0.22.	58
7.6. Audio signal for N ₂ -H ₂ jet flame with V _{jet} =500 m/s, N _{N₂} =0.294 and Φ _{co-flow} =0.22.	58
7.7. Audio signal for N ₂ -H ₂ jet flame with V _{jet} =500 m/s, Y _{N₂} =0.431 and Φ _{co-flow} =0.22.	59
7.8. Ignition frequency as a function of Y _{N₂} for V _{jet} =300 m/s from audio recordings.	60
7.9. Ignition frequency as a function of Y _{N₂} for V _{jet} =400 m/s from audio recordings.	61
7.10. Ignition frequency as a function of Y _{N₂} for V _{jet} =500 m/s from audio recordings.	61
7.11. Ignition frequency as a function of Y _{N₂} for V _{jet} =300 m/s and Φ _{co-flow} =0.20 from audio recordings.	62
7.12. Ignition frequency as a function of Y _{N₂} for Φ _{co-flow} =0.20 from audio recordings.	64
7.13. Ignition frequency as a function of Y _{N₂} for Φ _{co-flow} =0.22 from audio recordings.	64
7.14. Ignition frequency as a function of Y _{N₂} for Φ _{co-flow} =0.24 from audio recordings.	65
7.15. Ignition frequency as a function of Y _{N₂} for Φ _{co-flow} =0.25 from audio recordings.	65
7.16. Ignition frequency as a function of Y _{N₂} for Φ _{co-flow} =0.27 from audio recordings.	66
7.17. Ignition frequency as a function of Y _{N₂} for V _{jet} =300 m/s from high speed video	69
7.18. Ignition frequency as a function of Y _{N₂} for V _{jet} =400 m/s from high speed video	69
7.19. Ignition frequency as a function of Y _{N₂} for V _{jet} =500 m/s from high speed video	70
7.20. Comparison of results from audio recordings and high speed video. Ignition frequency as a function of Y _{N₂} for V _{jet} =300 m/s.	71

7.21. Comparison of results from audio recordings and high speed video. Ignition frequency as a function of Y_{N_2} for $V_{jet}=400$ m/s. 71

7.22. Comparison of results from audio recordings and high speed video. Ignition frequency as a function of Y_{N_2} for $V_{jet}=500$ m/s. 72

List of Tables

2.1.	Hydrogen properties compared with methane and iso-octane.	17
2.2.	Mixture properties for hydrogen-air, methane-air and iso-octane-air	19
6.1.	$\Phi_{co-flow}$ with the corresponding calculated temperatures. . .	44
7.1.	Random time step uncertainty for the two chosen cases with $V_{jet}=300$ m/s and $\Phi_{co-flow}=0.22$	74
7.2.	Random counting uncertainty of $V_{jet} = 300$ m/s and $\Phi = 0.20$.	75
7.3.	Results from calculation of systematic uncertainty for a flame with $V_{jet}= 400$ m/s and $\Phi_{co-flow}=0.22$	76
7.4.	Random, systematic and total uncertainty estimate for a flame with $V_{jet}=400$ m/s and $\Phi_{co-flow}=0.22$	77
7.5.	Random uncertainty of the high speed video results for a flame with $V_{jet}=300$ m/s and $\Phi_{co-flow}=0.20$	78
A.1.	Audio results, $V_{jet}=300$ m/s.	87
A.2.	Audio results, $V_{jet}=300$ m/s, continued.	88
A.3.	Audio results, $V_{jet}=400$ m/s.	89
A.4.	Audio results, $V_{jet}=400$ m/s, continued.	90
A.5.	Audio results, $V_{jet}=400$ m/s, continued.	91
A.6.	Audio results, $V_{jet}=500$ m/s.	92
A.7.	Audio results, $V_{jet}=500$ m/s, continued.	93
A.8.	Video results, $V_{jet}=300$ m/s.	93
A.9.	Video results, $V_{jet}=400$ m/s.	94
A.10.	Video results, $V_{jet}=400$ m/s, continued.	95
A.11.	Video results, $V_{jet}=500$ m/s.	96
B.1.	Calculation of systematic uncertainty for a flame with $V_{jet}=400$ m/s and $\Phi_{co-flow}=0.22$	99
C.1.	Calculation of random counting uncertainty for $V_{jet} = 400$ m/s and $\Phi = 0.22$	101

List of Tables

C.2. Calculation of time step uncertainty for $V_{jet} = 400\text{m/s}$ and
 $\Phi = 0.22$ with $t = 40\text{s}$ 101

1. Introduction

Energy from combustion of fossil fuels is by far the most important energy source in the world, contributing to about 90% of the worlds total energy use. More than 40 % of the worlds electricity comes from the burning of coal and the transport system relies almost entirely on combustion of liquid fossil fuels. Industrial processes also rely heavily on combustion [IEA, 2008] [Turns, 2006].

While the consumption of fossil fuels is increasing, the products of combustion are recognized as a severe source of environmental damage. About 95% of the worlds air pollution comes from combustion of fossil fuels. The major pollutants are unburned hydrocarbons, nitrogen oxides, carbon monoxide, sulfur oxides and particulate matter. The major combustion product from combustion of hydrocarbon fuels are carbon dioxide and water. Carbon dioxide is considered a significant greenhouse gas, and concerns of a global greenhouse effect are being raised [Warnatz et al., 2001, Ch. 17] [Ertesvåg, 2000].

The combustion products are almost always deposited into the atmosphere. This is a problem for the air quality and climate as combustion is increasing worldwide. Global warming, harmful pollutant emission and increased energy costs have driven initiative to develop cleaner and more fuel efficient combustion systems. Researchers all over the world are working on finding effective ways to reduce the emissions with respect to cost, technical feasibility and retrofit implementation. Investing in renewable energy sources like wind, solar energy and biomass with the aim to phase out fossil energy sources seems like the obvious answer, but taking into account economical considerations and the time available for scale-up make these solutions unlikely to solve the problem soon enough.

One possible way of reducing the emissions from coal combustion is by gasification of the coal and combustion of the product; hydrogen, H_2 . Gasification of coal is the reaction between coal, oxygen and steam to produce a mixture of hydrogen and carbon monoxide (syngas). The syngas then

1. Introduction

reacts further with water vapor to form a mixture of hydrogen and carbon dioxide, from where the carbon dioxide can be removed and sequestered. The hydrogen can be burned in gas turbines with water and compounds containing nitrogen and oxygen as the only products, see fig. 1.1. State of the art technology for gas turbines apply combustors that are designed for natural gas and/or oil and will have to be redesigned to work optimally, safely and effectively with hydrogen as a fuel [Ströhle and Myhrvold, 2007].

Combustion of any fuel in air at high temperatures will result in NO_x formation. NO_x is a collective term which refers to nitric oxide, NO , and nitrogen dioxide, NO_2 . NO_x production is highly dependent on temperature, residence time, mixedness and pressure. NO_x is a major contributor of photochemical smog and ozone in the urban air. In addition, NO_x is a participant in a chain reaction which removes ozone from the stratosphere and as a result, the ultraviolet radiation reaching the surface of the earth is increased [Warnatz et al., 2001]. Furthermore, NO_x is one of the major contributors to acid rain which is harmful to plants, aquatic animals and buildings [Pello, 2008].

The gas turbines designed for natural gas often operate in a premixed mode. Premixed combustion means that the fuel and oxidizer are mixed before the combustion occurs. This reduces the NO_x formation. In most of today's practical combustors premixed combustion is applied because premixed combustion is superior to non-premixed combustion when it comes to pollution control of NO_x among others [Warnatz et al., 2001]. The focus of this research is on how hydrogen can be premixed or partially premixed to avoid unsafe operating conditions and reduce the NO_x emissions.

Working with hydrogen as a fuel is challenging compared with other more conventional fuels like natural gas. The major challenges today's researchers encounter when working with hydrogen combustion are the high flame speed, the high flame temperature and difficulties in stabilizing the flame. The hydrogen molecule is light and has high molecular and thermal diffusivity. It is a highly reactive molecule with a large flammability range. This leads to the high flame speed and danger of autoignition and flashback [Ströhle and Myhrvold, 2007]. Detailed knowledge about the combustion characteristics of hydrogen is essential in order to overcome these challenges.

There are two methods of obtaining this knowledge, computer modeling and laboratory experiments. Combustion modeling is becoming more and more widely used and Computational Fluid Dynamics has taken over the role of laboratory experiments to an increasing extent due the increase of

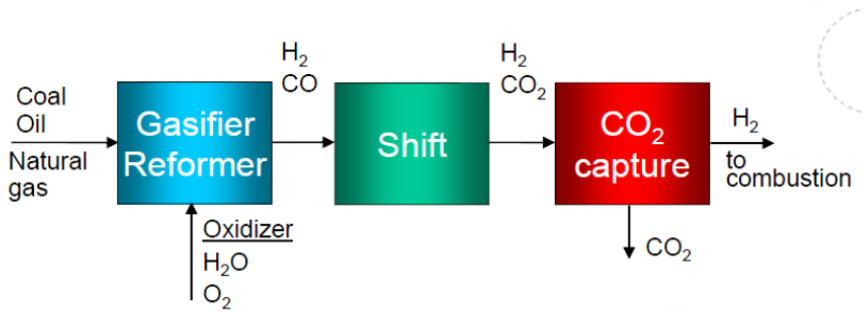


Figure 1.1.: Gasification of fossil fuels.

CPU-speed, memory and storage capacity the last years, as well as the fact that it is less expensive and time consuming than laboratory experiments. However, laboratory experiments are still needed for the evaluation and verification of the models and to provide new information about the physics of combustion and fluid motion.

The focus of this report is experimental investigation of hydrogen combustion at Berkeley's Vitiated Co-flow Burner (VCB). The VCB is a laboratory setup consisting of a central jet surrounded by a co-flow generated by lean premixed combustion of hydrogen and air. The fuel of the jet flame consists of a mixture of hydrogen and nitrogen. This configuration is used because it resembles the hot environment found in most practical combustion systems where the hot combustion products are recirculated to enhance flame stability.

This report presents an experimental investigation of intermittent flame blowout and re-attachment of the Vitiated Co-flow Burner jet flame at atmospheric pressure and varying N_2 - H_2 compositions, jet velocities and co-flow temperatures. The report first presents the most important theory of turbulent combustion followed by a presentation of the most relevant previous work. The report then presents the experimental setup of the VCB followed by the objectives of the experiments. The methodology is described and the results are presented and discussed. An uncertainty analysis is performed on selections of the results. Conclusions are drawn and suggestions for further work are given.

2. Theory

2.1. Turbulence

Turbulence is a common phenomenon in our everyday life. It can be observed in water flowing in a river or waterfall, in the smoke from a chimney and in the buffering of a strong wind. Turbulent flow is the most common type of flow in practical devices such as internal combustion engines, gas turbines, furnaces and boilers. The flows in pumps, compressors, pipelines are also usually turbulent.

Although most fluid flows occurring in nature and engineering applications are turbulent it is difficult to find a complete definition of the phenomenon. Turbulent flow can be defined as a stochastic fluctuating, non stationary, three dimensional rotating flow with strong dissipative and diffusive properties. Mixing in turbulent flows is much stronger than the mixing due to laminar (molecular) action. Turbulent eddies move about in three dimensions causing rapid diffusion of mass, momentum and energy. Heat transfer and friction are much larger than in laminar flows. Turbulence results from fluid mechanical instabilities when the viscous forces are not strong enough to damp the perturbations in the flow, typical for high Reynolds numbers [Turns, 2006][Pope, 2000][White, 2006]. The Reynolds number is a dimensionless number correlating the viscous behavior of all Newtonian fluids¹ and is defined as follows:

$$\text{Re} = \frac{uL}{\nu} \quad (2.1)$$

where u and L are characteristic velocity and length scales of the flow, respectively, and ν is the kinematic viscosity [White, 2008].

Figure 2.1 illustrates a typical velocity profile for turbulent flow. The horizontal line shows the mean velocity denoted by $\langle V \rangle$. It can be seen

¹For a Newtonian fluid the shear stress τ , is proportional to the velocity gradient according to the equation $\tau = \mu \frac{du}{dy}$ where μ is the dynamic viscosity and u is the velocity [White, 2008].

2. Theory

that the velocity $V(t)$ varies in an irregular pattern. It displays significant fluctuations and the time history exhibits variations on a wide range of time scales. The fluctuations of the velocity, u' , occur because of vortices generated by shear within the flow [Warnatz et al., 2001, ch. 13].

In turbulent reacting flows there are also frequently large random fluctuations in temperature, density and species concentration [Pope, 2000] [Jakobsen, 2008]. A reactive flow is a flow where chemical reactions occur. In addition to the conservation equations for mass, momentum and energy, an equation for the conservation of species is needed to fully describe the flow.

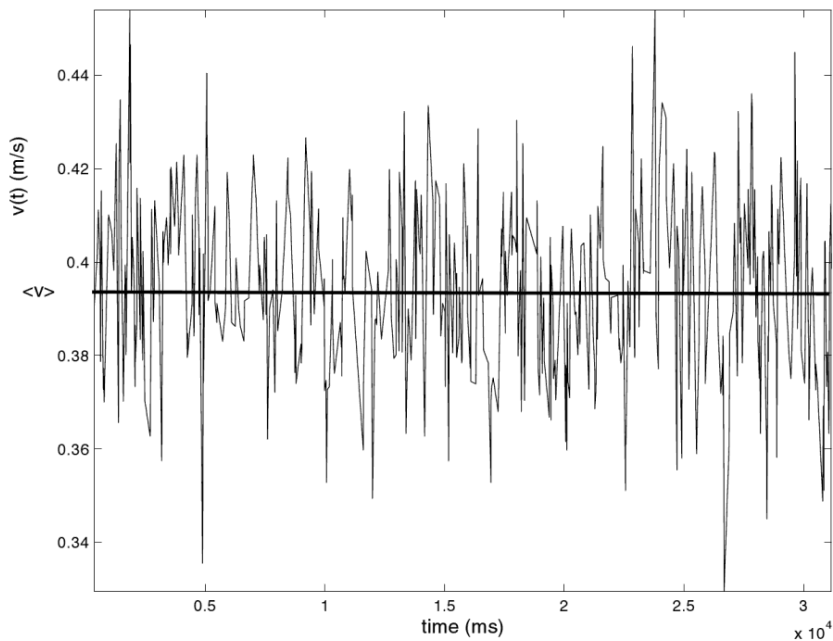


Figure 2.1.: Typical turbulent velocity signal recorded by a laser Doppler anemometer [Jakobsen, 2008].

A turbulent eddy is a macroscopic fluid element in which the microscopic element composing the eddy behave in some way as a unit. A vortex embedded in a fluid flow is considered an eddy. A turbulent flow contains many

eddies with a variety of different sizes and vorticity². A fully developed turbulent flow consist of a wide range of length scales, i.e., eddy sizes, from the largest determined by the geometry of the flow to the smallest determined by viscosity. The Reynolds number gives a measurement of the ranges of scales present, the larger the Reynolds number, the larger the range of sizes from the smallest eddy to the largest. It is this large range of length scales that makes the calculations of turbulent flows intractable [Turns, 2006, Ch. 11].

²The vorticity is the curl of the velocity and is twice the rotation of the fluid [Pope, 2000].

2.2. Combustion

The term combustion is usually used to refer to an exothermic reaction between a fuel and an oxidizer. The oxidizer is usually air and the fuel can be coal, oil, gas, or wood to mention a few. For combustion to occur the fuel and oxidizer must be mixed at molecular level and the temperature must be high enough for the reaction to occur. Combustion can occur in a flame or non-flame. A flame is defined as a self-sustaining propagation of a localized combustion zone. A flame can be divided into two zones, the preheat zone and the reaction zone. In the preheat zone little heat is released while in the reaction zone the bulk of the chemical energy is released [Turns, 2006].

Flames can be categorized in premixed and non-premixed flames. In premixed combustion the reactants are mixed at a molecular level before the burning occur and in non-premixed combustion the the mixing of the fuel and oxidizer occur during the combustion process itself. Further on these categories can be divided into turbulent and laminar flames [Warnatz et al., 2001, Ch. 1].

2.2.1. Premixed Combustion

Turbulent premixed flames are of tremendous practical importance, being encountered in many useful devices such as the spark-ignition engine, stationary gas-turbine engines and industrial gas burners.

A premixed flame is a flame where the reactants are mixed before the reaction occurs. It is characterized by the equivalence ratio, Φ , defined as

$$\Phi = \frac{m_f/m_a}{(m_f/m_a)_{st}} \quad (2.2)$$

where m_f is the amount of fuel, m_a is the amount of air and the subscript st represents the stoichiometric condition for complete consumption of the mixture. $\Phi < 1$ corresponds to a lean mixture (excess of air) and $\Phi > 1$ corresponds to a rich mixture (excess of fuel). $\Phi = 1$ corresponds to a stoichiometric mixture [Turns, 2006, Ch. 2]. The equivalence ratio affects the flame temperature. The flame temperature is at its maximum at slightly rich mixtures and fall off on either side [Turns, 2006, Ch. 8]. This means that for a lean mixture the flame temperature will increase with increasing equivalence ratio while for a rich mixture a premixed flame will show the opposite trend.

Flame Speed

The flame speed is one of the most important characteristics in premixed combustion because it dictates the flame shape as well as important flame-stability characteristics such as blowout and flashback. The flame speed of a premixed flame is defined as the speed an observer “riding” the flame would experience the unburned mixture approaching at [Turns, 2006, Ch. 12].

The laminar flame speed of a fuel-air mixture is dependent on pressure and temperature. It is strongly dependent on the temperature because the reaction rate is an exponential function of the temperature which causes the flame speed to increase with increasing temperature of the unburned reactants or surroundings. The turbulent flame speed is also dependent on the character of the flow, the geometry and the history of the flame as well as the mixing properties of the flow [Verhelst and Walner, 2009] [Turns, 2006, Ch. 12].

2.2.2. Non-Premixed Combustion

A non-premixed flame, traditionally known as “diffusion flame”, is a flame where the fuel and oxidizer are not mixed before the combustion occurs, thus the mixing and combustion occur simultaneously. Fuel and oxidizer diffuse to the flame front due to the gradients caused by the chemical reaction. The flame is fixed to the interface between the oxidizer and fuel because the flame cannot propagate into the oxidizer without fuel and vice versa. The products and energy diffuse away from the flame front and into the fuel and oxidizer [Warnatz et al., 2001, Ch. 9].

In the majority of practical combustion systems the fuel and oxidizer are separate before they are introduced into the burner. Turbulent non-premixed flames are employed because such flames can easily be controlled. Turbulent non-premixed flames are found in diesel engines, steam boilers, aircraft gas-turbines, furnaces and hydrogen-oxygen rocket motors. Non-premixed combustion is often used because of safety considerations [Warnatz et al., 2001]. The chemical reactions between the oxidizer and fuel occur at a molecular level. Therefore the mixing between the fuel and oxidizer must occur before the combustion can take place. The chemical reactions are often fast and the mixing process is the limiting step for the burning rate rather than the chemical kinetics. Therefore great flame stability can be achieved for

2. Theory

non-premixed flames and many combustion application use non-premixed flames due to this feature [Pello, 2008].

There are many different types of non-premixed flames for example jet flames, liquid-fuel sprays in diesel engines, flames stabilized by strong recirculation zones in industrial boilers and flames stabilized by bluff bodies in turbojet afterburners. This report mainly concerns turbulent jet flames which will be explained in the following section.

Turbulent Non-Premixed Jet Flames

In a jet flame the fuel exits from a jet port into a surrounding fluid. When the gas velocity is low the flame is laminar. As the gas velocity increases the flame reaches a transition point at a critical Reynolds number and the flame becomes turbulent at high velocities. Non-premixed jet flames of hydrocarbon fuels are generally more luminous than premixed flames because some soot is present within the flame [Turns, 2006, Ch. 13].

The fuel in a jet flame flows along the flame axis. The fuel diffuses radially outwards while the oxidizer diffuses radially inwards. The surface of the flame is normally defined to exist at the location where the fuel and oxidizer meet at stoichiometric proportions which corresponds to an equivalence ratio of unity [Turns, 2006, Ch. 9].

At low flow rates the base of the flame lies close to the jet port (within a few millimeters) and the flame is said to be an *attached* flame. By increasing the flow rate the flame will at some point no longer be attached to the burner port but be lifted at a distance above the port. This condition is called *liftoff* (see fig. 2.2). By increasing the jet flow rate further the liftoff height will increase until the flame blows out. This is called *blowout*. The two conditions, liftoff and blowout, are critical conditions related to flame stabilization [Turns, 2006, Ch. 13].

The distance between the port and the base of the flame is called the *liftoff height*. Figure 2.2 shows the schematics of a lifted jet flame. When the flame is lifted the reactants will be partially premixed before the reaction occurs. This is called a partially premixed flame [Ertesvåg, 2000, Ch. 10]. Pitt [Pitt, 1989] gives a good summary of liftoff and blowout of turbulent jet flames where the theoretical and experimental work done to predict liftoff and blowout behaviors is presented.

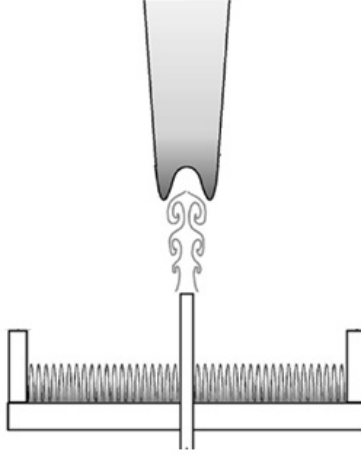


Figure 2.2.: Lifted jet flame.

In a non-premixed jet flame a mixture fraction ξ can be defined as follows:

$$\xi = \frac{Z_i - Z_{i2}}{Z_{i1} - Z_{i2}} \quad (2.3)$$

where Z_i is an element mass fraction, Z_{i1} is the element mass fraction in stream one (the jet stream) and Z_{i2} is the element mass fraction in stream two (the air stream surrounding the jet). The advantage of using the mixture fraction is that by computing the mixing of one element the mixing of everything else can be computed [Turns, 2006, Ch. 13] [Warnatz et al., 2001, Ch. 14].

From the mixture fraction the scalar dissipation rate, χ , can be defined as follows:

$$\chi = 2D \left(\frac{\partial Z}{\partial x_j} \right)^2 \quad (2.4)$$

where D is the diffusion coefficient and Z is the mixture fraction [Chen and Axelbaum, 2005]. Physically, the scalar dissipation rate can be interpreted as the mixing rate or as the rate at which scalar fluctuations are destroyed [Su, 1998]. In turbulent flows the scalar dissipation is analogous to the dissipation of the turbulent energy, ϵ . The temperature in a non-premixed flame depends strongly on the scalar dissipation rate. The scalar

2. Theory

dissipation rate is related to the rate of strain which is the gradients in axial velocity [Chen and Axelbaum, 2005].

Triple Flame

A partially premixed flame can form a triple flame when a partially mixed layer is formed between the fuel and oxidizer. This can happen in a lifted flame because the fuel mixes with the air in the region between the port of the jet tube and the flame base. The triple flame consists of two regions of premixed flames, one lean and one rich. In the region between these two regions there is a thin “tail” where there is a stoichiometric non-premixed flame. The triple flame speed is about three times the laminar flame speed [Pello, 2008][Cabra, 2003].

2.2.3. Flame Stabilization

Flame stabilization is of fundamental importance to turbulent combustion design. This is important due to issues of safety, efficiency and emission control. A stable flame is a flame that is anchored at a desired location and is resistant to flashback, liftoff and blowout over the operating range of the device [Turns, 2006, Ch. 12]. Flashback is the condition when the flame propagates upstream of the desired location of the flame. In premixed combustion flashback can occur when the local flame speed is larger than the mean flow velocity. The flame will propagate into the mixing section where combustion is unwanted. This might result in an explosion.

The essential principle in stabilizing a flame in a turbulent flow is that the local turbulent flame speed matches the local mean flow velocity [Turns, 2006, Ch.8]. Flame stabilization theory usually highlights local ignition, flame propagation, extinction and re-ignition as the important factors controlling stability.

Flame Ignition

Ignition is the time-dependent process starting with reactants and resulting in a steadily time-independent burning flame. Different forms of ignition are induced ignition (e.g. spark plug), thermal ignition and autoignition. In thermal ignition processes the temperature increases at once while for

autoignition the temperature increase occurs after a certain ignition-delay time (induction time). The ignition-delay time depends strongly on the temperature. The ignition-delay time will decrease with increasing temperature [Warnatz et al., 2001, Ch. 10]. Autoignition occurs when the heat generated by the reaction is greater than the heat transfer away from the mixture. This leads to a self-heating process and the temperature of the mixture increases until the mixture ignites [Pello, 2008]. Autoignition is a process of great importance to fire safety and internal combustion engines. For autoignition to take place, the reactants must be mixed and two independent quantities must be fulfilled: the critical heating period and the critical temperature [Toong, 1983, Ch. 8].

Flame Extinction

Extinction is defined from the limiting case where reactants proceed through the stoichiometric zone without burning. In a steady non-premixed flame the heat released in the reaction zone is balanced by the heat removed by diffusion and convection

[Vervisch and Poinso, 1998]. A non-premixed turbulent jet flame is extinguished (blown out) when the decrease of temperature due to the convective and diffusive heat removal is increasing while the heat generated from chemical reactions in the flame zone is decreasing due to the reduced reaction rate and due to the reduced residence time in the flame zone [Warnatz et al., 2001, Ch. 14]. In other words, when the chemistry is too slow or the scalar dissipation rate is too high, the chemical processes are not able to keep up with the large heat losses and extinction occurs [Vervisch and Poinso, 1998].

2.3. Gas Turbine Combustion and NO_x Control

Gas turbines are used to power aircraft and in stationary power system generating electricity [Turns, 2006, Ch. 12]. The focus of this report is on stationary gas turbines. Figure 2.3 shows the schematics of a gas turbine with a non-premixed combustor design. Figure 2.4 shows the schematics of a two staged gas turbine that utilizes premixed combustion.

A challenge when it comes to gas turbine combustion is to achieve easy ignition, wide burning range, high combustion efficiency and minimum pol-

2. Theory

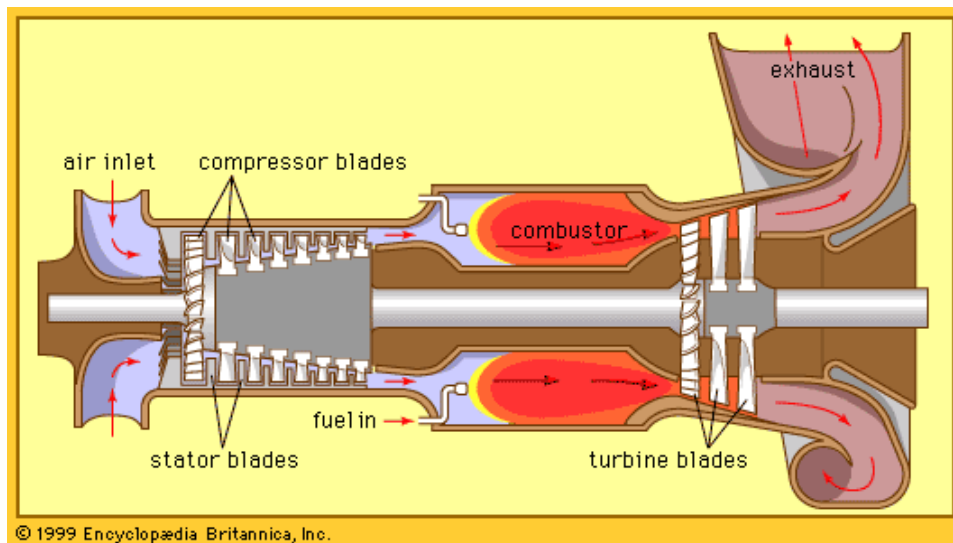


Figure 2.3.: Schematics of a gas turbine with a non-premixed combustor design.

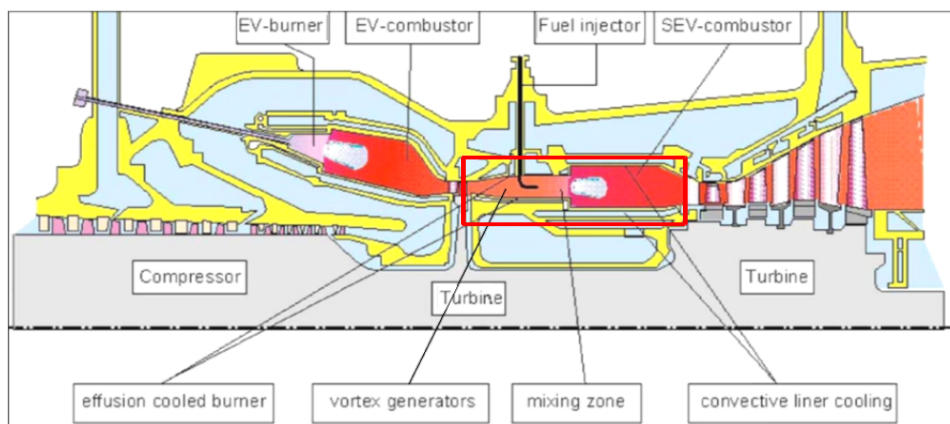


Figure 2.4.: Schematics of a two staged gas turbine with a premixed combustor design. The second stage of the gas turbine is shown in the red square.

lutant emissions. When hydrogen is used as a fuel, the only pollutant is, as mentioned in the introduction, NO_x [Lefebvre and Ballal, 2010]. Therefore the development of gas turbines fueled on hydrogen is focused on safe operation and low NO_x emissions.

For general combustion in stationary gas turbines one of the three following methods to reduce NO_x emissions is usually applied [Chiesa et al., 2005]:

- Premixed combustion including catalytic combustion.
- Removal of NO_x from exhaust gas.
- Fuel dilution, mostly by steam, water or nitrogen.

For gas turbines with natural gas as a fuel the first technique is usually preferred. However, with hydrogen as a fuel pre-mixing is not favored due to the high flammability limits of hydrogen. This method cannot be safely used because the high reactivity of hydrogen with air under typical gas turbine conditions might lead to an explosion (see section 2.2.3) [Chiesa et al., 2005]. Non-premixed combustion is the safest combustion mode to use in order to avoid flashback. However, by the use of non-premixed combustion the stoichiometric flame temperature is representative of the actual flame temperature. The stoichiometric flame temperature is strictly related to the NO_x formation rate. Hydrogen has a stoichiometric flame temperature of 2483 K which would lead to unacceptably high NO_x emissions [Lefebvre and Ballal, 2010].

The second technique for reducing NO_x emissions, removal from exhaust gas, includes selective catalytic reduction by means of ammonia injection [Heck et al., 2009]. This method can be used to remove NO_x from the exhaust gas of a hydrogen fueled gas turbine. However, the costs and size related to the high NO_x formation due to the high flame temperature would be excessively high [Chiesa et al., 2005].

The preferred method for reducing NO_x emissions from hydrogen combustion is therefore fuel dilution. Fuel dilution facilitates partially premixed combustion by increasing the momentum of the fuel jet thereby allowing the flame to detach from the nozzle. Some air will mix with the fuel and the combustion will be partially premixed. If the hydrogen being used comes from gasification of heavier hydrocarbons after decarbonization of the syngas, nitrogen will be present at large quantities [Chiesa et al., 2005]. By diluting the hydrogen with nitrogen and burning it in a partially premixed manner it is possible to reduce the NO_x emissions to an acceptable level.

2. Theory

For NO_x to be formed, both time and high temperature are necessary. The typical combustor residence time is around 5 ms. The residence time denotes how long time a reactant spends in the reaction zone. The formation of NO_x increases with an increase of the residence time [Lefebvre and Ballal, 2010].

To reduce the NO_x emissions the reaction temperature must be lowered and the residence time must be kept to a minimum. This is done by burning the fuel in a partially premixed manner, ensuring a lower peak temperature and a smaller flame which leads to a shorter residence time for the reactants in the high temperature zone.

2.4. Hydrogen Fundamentals

Hydrogen has some special properties compared to other fuels. Some of these properties are positive features and some represent an extra challenge. Table 2.1 lists some properties of hydrogen compared to methane and iso-octane. Hydrogen is a light molecule with low density and high mass diffusivity. It has a low ignition energy, short minimum quenching distance and a wide range of flammability limit, ranging from as lean mixtures as for $\Phi = 0.14$ to very rich mixtures of $\Phi = 10$ at atmospheric conditions. Both the lower and higher heating values of hydrogen are much higher than those for methane and iso-octane. Hydrogen has the highest energy-to-weight ratio of any fuel.

Table 2.2 lists some important mixture properties of H_2 -air mixtures at stoichiometry compared to stoichiometric methane-air and iso-octane-air mixtures. The laminar flame speed of H_2 is many times higher than that of other fuels (here by a factor of six) which is one of the main challenges with hydrogen as a fuel.

Table 2.1.: Hydrogen properties compared with methane and iso-octane at 300 K and 1 atm [Verhelst and Walner, 2009].

Property	Hydrogen	Methane	Iso-octane
Molecular weight [g/mol]	2.016	16.043	114.236
Density [kg/m^3]	0.08	0.65	692
Mass diffusivity in air [cm^2/s]	0.61	0.16	~ 0.07
Minimum ignition energy [mJ]	0.02	0.28	0.28
Minimum quenching distance [mm]	0.64	2.03	3.5
Flammability limits in air [vol %]	4-75	5-15	1.1-6
Flammability limits, Φ	10-0.14	2-0.6	1.51-0.26
Lower heating value [MJ/kg]	120	50	44.3
Higher heating value [MJ/kg]	142	55.5	47.8
Stoichiometric air-to-fuel ratio	34.2	17.1	15.0
Stoichiometric air-to-fuel ratio	2.387	9.547	59.666

By diluting hydrogen with nitrogen the laminar flame speed is greatly reduced. Figure 2.5 shows how much the laminar flame speed of lifted hydrogen jet flames is reduced by diluting hydrogen with 15 % and 25 % of nitrogen compared to pure hydrogen as a function of the mixture fraction, f , normalized by the stoichiometric mixture fraction f_{st} [Tacke et al., 1998].

2. Theory

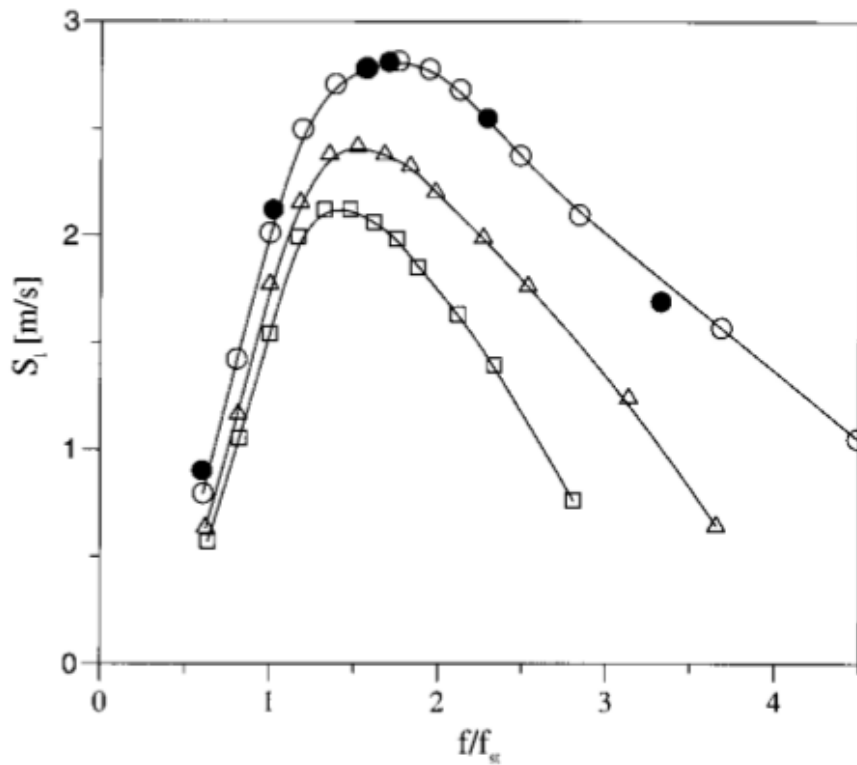


Figure 2.5.: Laminar flame speed of the fuel mixtures, \circ :100 vol.% H₂; \triangle :85/15 vol % H₂/N₂; \square :75/25 vol % H₂/N₂ [Tacke et al., 1998].

Table 2.2.: Mixture properties for hydrogen-air, methane-air and iso-octane-air at 300K, 1atm and stoichiometric mixture ($\Phi = 1$) [Verhelst and Walner, 2009].

Property	H ₂ -air	CH ₄ -air	C ₈ H ₁₈ -air
Volume fraction fuel (%)	29.5	9.5	1.65
Mixture density [kg/m ³]	0.850	1.123	1.65
Kinematic viscosity [mm ² /s]	21.6	16	15.2
Adiabatic flame temperature [K]	2390	2226	2276
Thermal conductivity [10 ⁻² W/mK]	4.97	2.42	2.36
Thermal diffusivity [mm ² /s]	42.1	20.1	18.3
Laminar flame speed, T=360 K, [cm/s]	290	48	45

Furthermore, hydrogen has a high flame temperature. As mentioned in section 2.2 the equivalence ratio affects the flame temperature. The following equation can be used to calculate the flame temperature, T , from a given equivalence ratio [Cabra, 2003]:

$$T = 2462(\Phi)^{0.69} \quad (2.5)$$

This equation is valid for equivalence ratios between 0.15 and 0.4.

The autoignition temperature of hydrogen at atmospheric conditions is 858 K which is relatively high compared to other fuels [White et al., 2006]. Another special feature of hydrogen flames is the fact that they are not very luminous due to the absence of soot. A premixed hydrogen flame is invisible and a non-premixed flame is barely visible burning with a pale blue color [Züttel et al., 2008]. This leads to challenges with regard to diagnostics of hydrogen combustion and it can also be a safety issue.

2.5. Measurement Uncertainty

All measurements of a variable contain inaccuracies. In measurement systems there will always be some deviations between the value measured and the actual value. The error of a measurement is defined as the difference between the true value and the measured value:

$$\text{Error} = \text{measured value} - \text{true value}$$

The error of a measurement is usually unknown and it is normally not possible to know what the error is. If the true value of the property being measured was known then there would be no need to make the measurement. What can be done is to estimate the uncertainty of the measurement. The uncertainty is an estimate of the limits of error in the measurement with some level of confidence. The level of confidence is usually 95%. Errors in experiments can be divided into two categories, random errors and systematic errors [Wheeler and Ganji, 2004]. These will be explained in the following sections.

2.5.1. Random Uncertainties

Random errors leads to several different results if the same experiment is repeated several times. The random errors are caused by a lack of repeatability in the output of the measuring system. An average of the random error is usually normally distributed. By multiple repetitions of the experiment the influence of random errors may be reduced.

The standard deviation of the sample groups is an expression of random error. The expression for the standard deviation, S_x , is as follows:

$$S_x = \left[\frac{1}{n-1} \sum_{i=1}^n (x_i - \bar{x})^2 \right]^{\frac{1}{2}} \quad (2.6)$$

where x_i is a given measurement, n is the number of measurements and \bar{x} is the mean of x determined by the following equation:

$$\bar{x} = \frac{\sum_{i=1}^n x_i}{n} \quad (2.7)$$

The Student's t distribution can be used to find the uncertainty by the use of a coefficient, t , that is given for a given confidence level (usually 95%) and degrees of freedom ($\nu = n - 1$). The Student's t distribution is used in cases of small samples [Wheeler and Ganji, 2004]. The random uncertainty, $P_{\bar{x}}$ can be determined from the following equation:

$$P_{\bar{x}} = \pm t \frac{S_x}{\sqrt{n}} \quad (2.8)$$

where $\frac{S_x}{\sqrt{n}}$ is the estimate of the standard deviation of the mean and t is the Student's t coefficient. Estimations of random uncertainties are dependent on the sample size.

2.5.2. Systematic Uncertainties

Systematic errors are repeatable, consistent errors. If the same measuring system is used several times in the same way to measure the same value of the variable, the systematic error will be the same each time [Wheeler and Ganji, 2004]. Systematic errors can be a result of wrong calibration, hysteresis or nonlinearities in the measurement instrument.

The equation used for calculating the systematic uncertainty for a result, R , that is a function of n measured variables, x_1, x_2, \dots, x_n , is as follows [Wheeler and Ganji, 2004]:

$$w_R = \left(\sum_{i=1}^n \left[w_{x_i} \frac{\partial R}{\partial x_i} \right]^2 \right)^{1/2} \quad (2.9)$$

where w_R denotes the systematic uncertainty in the result, w_{x_i} is the uncertainties in the variables and the partial derivative, $\partial R / \partial x_i$ is called the sensitivity coefficient of the result, R , with respect to the variable x_i . Equation 2.9 is known as the root of the sum of squares (RSS).

2.5.3. Estimate of Total Uncertainty

The total uncertainty of a measured variable is the interval around the best value of the measured variable within which it is expected that the true value lies within a given confidence level. To obtain the total uncertainty

2. Theory

the random uncertainty and the systematic uncertainty must be combined in the appropriate manner [Coleman and Steele, 1983]. This is done by using RRS in the following manner for the mean of x :

$$W_{\bar{x}} = (w_{R_x}^2 + P_{\bar{x}}^2)^{1/2} \quad (2.10)$$

where $W_{\bar{x}}$ is the total uncertainty of the result, w_{R_x} is the systematic uncertainty of the measured value, x , and $P_{\bar{x}}$ is the random uncertainty of the mean of x .

2.6. Signal Processing

Signal processing deals with operations on signals or analysis of signals. Signals of interest usually include sensory data from the real world like seismic vibrations, visual images and sound waves [Smith, 1997, Ch. 1]. This report deals with the processing of sound signals.

A signal can be processed in the time domain or the frequency domain. The Fourier transform is the mathematical relationship between these two domains and is used in signal processing to transform signals from the time domain to the frequency domain. In the time domain a plot shows how a signal changes with respect to time while the frequency domain shows how much of the signal lies within each given frequency over a frequency range. The signal represented in the time domain contains information of when something occurs and what the amplitude of the occurrence is. This is the simplest way for a signal to contain information. In the frequency domain the information represented is more indirect. By measuring frequency, phase and amplitude, information about periodic motions can be found like fundamental frequencies of the signal. The information in the frequency domain contains information on many points in the signal [Smith, 1997, Ch. 14]. The frequency domain contains the same information as the time domain but in a different form. If one domain is known, the other can be calculated [Smith, 1997, Ch. 8].

The Fourier transformer decomposes a function to a sum of Sine waves. The frequency domain represents the signal as a “spectrum” of frequency components. The Fourier transform, $X(\omega)$, of a signal, $x(t)$, is defined as follows:

$$X(\omega) = \int_{-\infty}^{\infty} x(t)e^{-i2\pi ft} dt \quad (2.11)$$

where i is the imaginary unit equal to the square root of -1, f represents the frequency and t represents the time.

In MATLAB (or other computer programming language) the continuous time fourier transformation cannot be calculated exactly. A Discrete Fourier Transformation (DFT) is calculated instead. The following equation is the definition of the Discrete Fourier Transformation:

$$X_k = \sum_{n=0}^{N-1} x_n e^{-\frac{2\pi i}{N} kn} \quad (2.12)$$

2. Theory

for $k = 0, \dots, N - 1$, where x_n is an array of complex time-domain data, n is an index of time steps, X_k is an array of complex frequency-domain data, k is an index of frequency spectral lines and N represents the size of the data arrays. The Fast Fourier Transformation (FFT) is one method for calculating the DFT that is very efficient and reduces computation time by hundreds compared to other methods [Smith, 1997]. The algorithm of the FFT and an explanation of how it works is beyond the scope of the present work.

2.6.1. Filters

Filters are applied to signals with two purposes: separation or restoration. Signal separation is applied to a signal that has been contaminated by interference, noise or other signals. Signal restoration is applied if a signal has been distorted in some way [Smith, 1997].

The most common filter in digital signal processing is the moving average filter. This filter is common because it is simple to understand and use and also works optimally for reducing random noise from a signal while retaining the sharp response. The moving average filter works in the following manner: a number of points from the input signal are averaged to produce each point in the output signal. Mathematically, this can be described by the following equation:

$$y[i] = \frac{1}{M} \sum_{j=0}^{M-1} x[i + j] \quad (2.13)$$

where $x[i]$ is the input signal, $y[i]$ is the output signal and M is the number of points used in the moving average (the filter width). In this equation only points on one side of the output sample are being used. The group of points from the input signal can also be chosen symmetrically around the output point. Increasing filter width will give increasing reduction of random noise but also decrease the sharpness of the signal. Of all linear filters to be used on signals in the time domain, the moving averaging filter produces the best noise reduction for a given edge sharpness [Smith, 1997, Ch. 15]. For more information on signal processing the reader is referred to [Smith, 1997].

3. Prior Work

Lifted non-premixed flames have been the subject of extensive research for more than 40 years. This is because lifted flames include fundamental mechanisms that are important for flame stabilization [Tacke et al., 1998]. The experimental setup of the jet flame surrounded by a hot co-flow has been frequently used in order to study jet flames in a hot environment. In the following sections the most important research done on turbulent jet flames in hot environments and still atmospheric air will be presented.

Cheng et al. [Cheng et al., 1992] investigated a lifted non-premixed hydrogen jet flame. The jet flame was formed by injecting fuel through a tube into still atmospheric air with a jet velocity of 680 m/s. At this jet velocity and with the diameter used in the experiment, the flame is lifted. Measurements were made of temperature, major species concentrations and hydroxyl radical concentration [OH]. These measurements were obtained with a “single” excimer laser for the first time. Measurements were made in the lifted zone, the slow recombination zone and the equilibrium zone. The results showed that in the center of the lifted flame base, fuel and oxidizer are premixed in a rich, low temperature and unignited condition. In the lifted flame zone combustion occurs at a position where unburned hydrogen and oxygen coexist in significant concentrations and OH exists in sub-equilibrium and super-equilibrium concentrations.

Ricardo Cabra [Cabra, 2003] developed a design for a Vitiated Co-flow Burner (VCB) and investigated hydrogen and methane flames on the VCB. The VCB design consisted of a jet surrounded by a perforated plate with 2000 small holes. This design was successful in providing a uniform and steady co-flow isolating the jet from the laboratory environment. Stabilization of hydrogen and methane was studied which resulted in the conclusion that lifted flames are stabilized by a combination of flame propagation, autoignition and localized extinction processes.

An investigation of lifted turbulent non-premixed flames of hydrogen and nitrogen diluted hydrogen was performed by Tacke et al. [Tacke et al., 1998].

3. *Prior Work*

The stabilization point of the flames was investigated by Raman-Rayleigh-laser induced fluorescence spectroscopy. It was shown that liftoff height has negligible influence on the flame length and the far regions of the jet. The results suggested a stabilization mechanism through large-scale turbulent structures. The existence of products upstream was also explained by large-scale structures and it was concluded that large-scale turbulent structures play a dominant role in the stabilization mechanism of lifted turbulent non-premixed flames.

The influence of the co-flow velocity on a lifted methane-air jet was investigated by Montgomery et al. [Montgomery et al., 1998] numerically in two dimensional computations. The numerical results corresponded well with experimentally obtained characteristics of lifted non-premixed flames. The results showed increasing flame liftoff height with increasing jet velocity and with increasing air co-flow velocity. The results of the computations imply that the liftoff height is insensitive to the small scale fluctuations and that liftoff is controlled by fluid dynamics and heat release more than the details of the chemistry.

A lifted turbulent hydrogen-air jet flame in a vitiated co-flow was investigated by Cabra and Myhrvold et al. [Cabra et al., 2002] experimentally and numerically. The laboratory experiments show spontaneous ignition of the flame when the co-flow is operating and the jet flow is turned on. This spontaneous ignition started at a far down-stream location. The numerical results from different combustion models used (PDF and EDC) predicted the liftoff height reasonably well.

The vitiated co-flow burner was used to study lifted methane-air flames by Cabra and Chen et al. [Cabra et al., 2005]. The liftoff height was found to vary almost linearly with jet velocity, co-flow velocity and co-flow temperature and it was found to be most sensitive to co-flow temperature.

Autoignition of hydrogen combustion in a turbulent heated air co-flow was studied experimentally by Markides and Mastorakos [Markides and Mastorakos, 2005]. They found four different combustion regimes with respect to ignition as follows:

- “No-ignition” regime: This regime was found for low air temperatures and high air velocities and high fuel velocities. Here no ignition occurs.
- “Random Spots” regime: For a range of higher air temperatures, lower air velocities and lower hydrogen velocities a statistically stable situation where instantaneous autoignition occurred in the form of random

spots was observed. These spots did not result in flashback nor an attached flame, but died out after a short period of time. The autoignition in this regime caused an intense noise with increased pitch and loudness as the temperature decreased or the velocity increased.

- “Flashback” regime: This regime was found for low air velocity and low hydrogen velocity and high air temperature. Here autoignition and flashback occurred subsequently. Flashback would occur from an ignition kernel randomly located in space with what seemed like a triple flame. This resulted in a normal jet flame.
- “Lifted Flame” regime: This regime was observed for even higher velocities and temperatures in which a stable lifted hydrogen flame is achieved. The observations in this regime coincided with the results from Cabra and Myhrvold et al. [Cabra et al., 2002] as described previously.

In the “Random Spots” regime it was found that the ignition delay time at the same air temperature increased with increasing air velocity. It was therefor concluded that the phenomena was not only chemically controlled and that turbulent mixing delays autoignition.

Wu et al. [Wu et al., 2009] investigated the stability of pure hydrogen flames as well as the effect of propane, methane and CO₂ addition in H₂ flames. The liftoff height was found to increase with increasing jet velocity. The results for liftoff heights for the pure hydrogen flame corresponded well with previous experimental results. Hydrocarbon addition to the gas showed lower liftoff velocities and higher liftoff heights than for pure hydrogen. Addition of propane to the hydrogen flame resulted in the lowest liftoff velocity and highest liftoff height of the three gases. Furthermore, addition of propane led to faster blowout of the flame than CO₂ addition.

North et al. [North et al., 2011] used the vitiated co-flow burner to study lifted hydrogen flames diluted with nitrogen in a co-flow of lean premixed hydrogen combustion. The experimental setup is the same as the one being used in the present study, see chapter 5. The liftoff height of several N₂-H₂ jet flames were measured. The liftoff height was investigated as a function of co-flow temperature, jet velocity and nitrogen dilution mole fraction. It was found that the liftoff height increased with increasing nitrogen dilution mole fraction and that at co-flow equivalence ratios up to 0.2 the liftoff height was seemingly unaffected by the co-flow temperature. When the data was normalized with respect to Reynolds number, the data collapsed

3. Prior Work

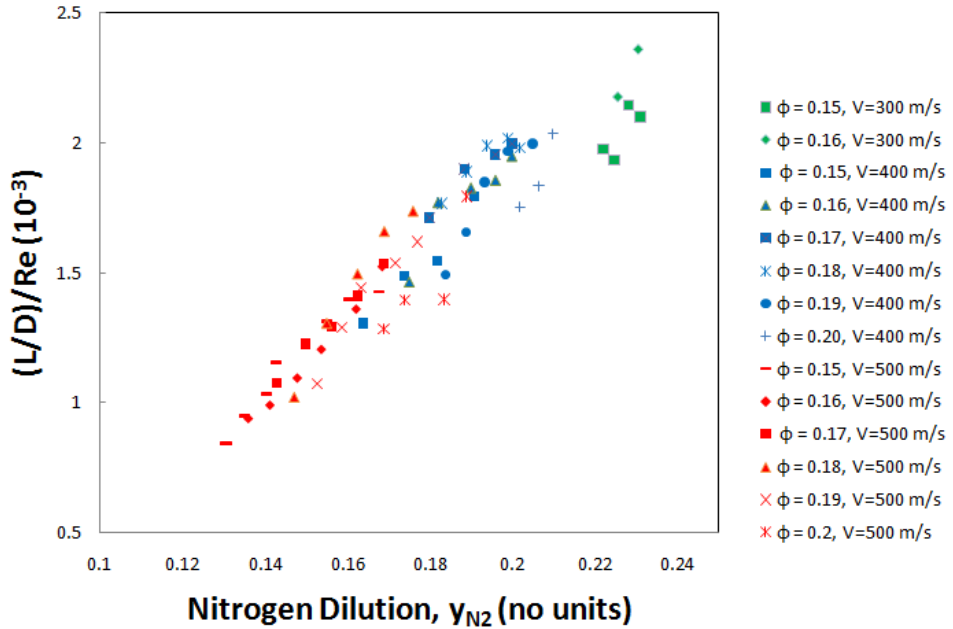


Figure 3.1.: Liftoff heights normalized by the Reynolds number [North et al., 2011].

to a straight line showing a linear dependency of the normalized lift-off height as a function of nitrogen dilution mole fraction, as can be seen in fig. 3.1. This indicates that the lift-off height is a function of fluid dynamic properties and not affected by the co-flow temperature.

The experiments by North et al. [North et al., 2011] resulted in a stability regime diagram for the N_2 - H_2 jet flame at three different velocities. Four different stability regimes were observed for the H_2/N_2 jet flame:

- Attached
- Lifted
- Unsteady
- Blown out

The stability regimes for the N_2 - H_2 jet flame were found as a function of co-flow equivalence ratio and nitrogen dilution mole fraction for three different jet velocities of 300, 400 and 500 m/s as can be seen in fig. 3.2. The flames

are attached for low nitrogen dilution mole fractions. With an increasing co-flow equivalence ratio the flames are attached for increasing nitrogen dilution mole fractions. For a low equivalence ratio, $\Phi < 0.15$, the co-flow is blown out. An equivalence ratio of 0.15 is the lower flammability range of a hydrogen-air flame at ambient pressure. The data points here are for a co-flow consisting of only air. In this region the flame becomes lifted when the nitrogen dilution mole fraction is increased to a certain value and after further increasing the nitrogen content the flame will at some point blow out.

When the co-flow equivalence ratio exceeds 0.2 the flame is no longer lifted but unsteady for a range of nitrogen dilution mole fractions. The unsteady region is characterized by a loud “popping” sound and intermittent chemiluminescence coming from the flame. At low nitrogen dilution mole fractions when the flame is just beginning to be unsteady the sound is noisy with low “pops” of low frequency. When the nitrogen dilution mole fraction is increased the sound becomes louder and the frequency of the “pops” increase. At high frequencies the flame sounds like a machine gun or a loud roar. When the nitrogen dilution mole fraction is further increased the sound becomes clearer with loud clearly distinguishable “pops” of low frequency.

Figure 3.2 shows two different unstable regions for $V_{jet}=500$ m/s. One where the flame oscillates between an attached flame and a lifted flame and one unstable region where the flame is blown out and subsequently re-attached as a lifted flame [North et al., 2011].

3. Prior Work

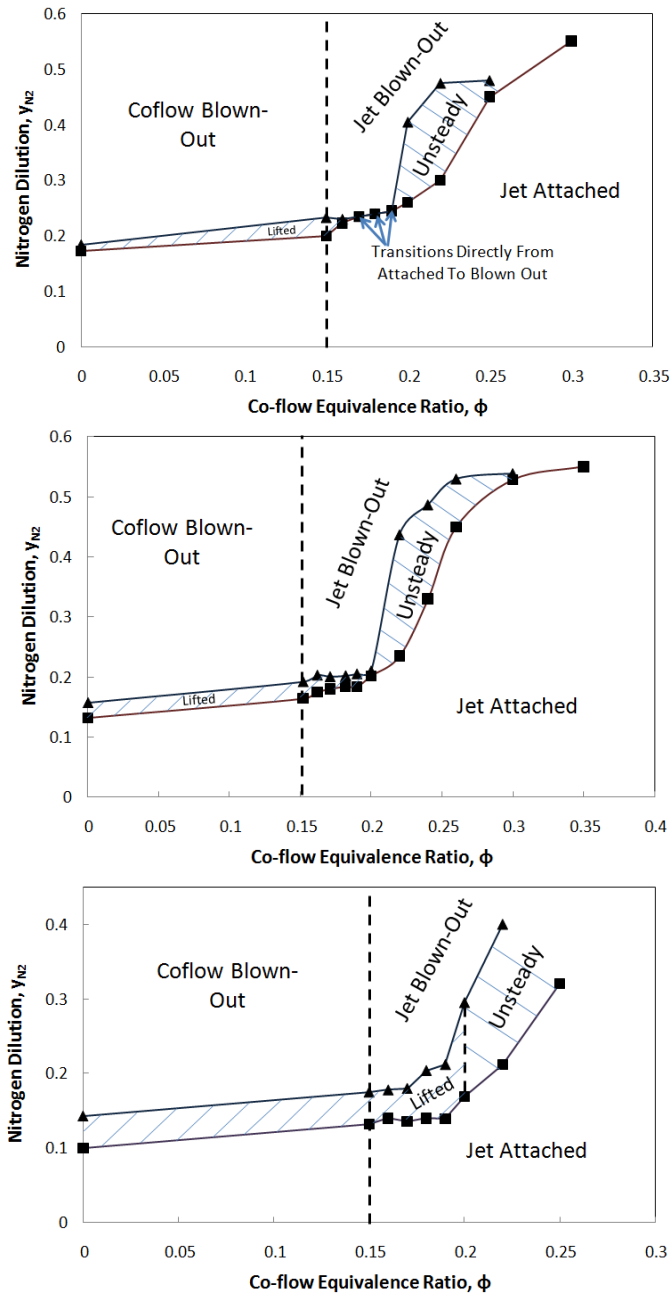


Figure 3.2.: Stability diagrams for N_2 - H_2 flames with jet velocities of $V_{jet} = 300$ (top), 400 (middle) and 500 m/s (bottom) [North et al., 2011].

4. Experimental Objective

The objective of the experiment is to investigate the statistical likelihood of autoignition of the N_2 - H_2 flame under varying conditions. The understanding of how and under what conditions a flammable mixture will autoignite is of tremendous importance for preventing unwanted ignition and initiating ignition at the proper time. Investigations of partially premixed hydrogen combustion is crucial in the effort of designing gas turbines for hydrogen as a fuel with low NO_x emissions.

As has been explained in section 2.2 the preferred method to ensure safe operation and low NO_x emissions in a gas turbine fueled by hydrogen is to burn the fuel in a partially premixed manner diluted with nitrogen. The VCB creates a hot environment which resembles the environment in the second stage of a gas turbine and makes it easy to adjust the surrounding temperature by adjusting the co-flow equivalence ratio. This gives an opportunity to study the effect of temperature on the N_2 - H_2 jet flame.

The objective of the research is to determine to what extent hydrogen can be premixed with products of lean hydrogen combustion without the risk of flashback. Better understanding of the combustion characteristics of hydrogen and hydrogen diluted with nitrogen is therefore important. Since the objective in practise is to prevent ignition in the mixing section of a gas turbine, it is the objective of this research to examine ignition and extinction during mixing. By studying lifted jet flames the fuel from the jet is being mixed with the surrounding co-flow before ignition. The present study will examine the frequency of ignition and blowout of nitrogen diluted hydrogen jet flows as a function of nitrogen dilution mole fraction, co-flow temperature and jet velocity. The frequency of the blowout-autoignition events will give an indication of the statistical likelihood of autoignition under the various conditions. As the frequency of ignition is reduced, the statistical likelihood of autoignition is correspondingly reduced. As it is increased the statistical likelihood of autoignition is correspondingly increased.

5. Experimental Apparatus

5.1. Berkeley's Vitiated Co-flow Burner

The concept of the Vitiated Co-flow Burner (VCB) was first presented in 1996 at the 1st International Workshop on Measurement and Computation of Non-premixed Turbulent Flames in Naples, Italy. The purpose of the VCB is to resemble the hot environment typical of practical combustors like in the the second stage combustor of a gas turbine. Advanced combustors usually operate at high temperature and pressure to facilitate reaction, increase efficiency and reduce emissions. Combustion chambers utilize recirculation of the hot exhaust gas to provide this hot environment. The reactants mix with a mixture of oxygen, nitrogen and hot reaction products. This mixture of air and hot reaction products is referred to as *vitiated* air. The advantages of studying lifted jet flames with this configuration are the following:

- The lifted flame entrains air before it ignites. This is similar to what happens during mixing in gas turbines.
- The study of lifted flames facilitates understanding of turbulence-chemistry that occur during combustion.
- The co-flow makes it easy to adjust the surrounding temperature.
- Numerical modeling is facilitated. Liftoff height is easily measured and encompasses a lot of combustion parameters. If a model can predict liftoff and liftoff height for a broad set of conditions this is a good way to verify the model.

The VCB used in the present work was developed as a part of the work of Ricardo Cabra [Cabra, 2003]. The VCB has been scaled down. A schematic of the VCB can be seen in fig. 5.1. The vitiated co-flow burner was designed with the objective of decoupling the detailed fluid mechanics from the chemical kinetics to facilitate the modeling and at the same time gain insight in the turbulence-flame interaction in a hot environment [Cabra, 2003]. The

5. *Experimental Apparatus*

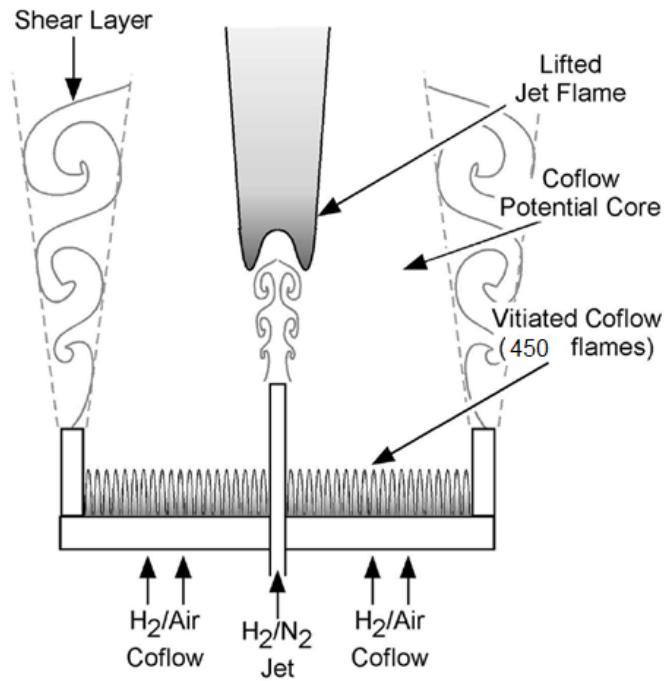


Figure 5.1.: Schematics of the Vitiated Co-flow Burner [North, 2010].

5.1. Berkeley's Vitiated Co-flow Burner

simplified coaxial configuration is a two-dimensional flow and for simple fuels like hydrogen and methane this configuration is suitable for numerical investigation. In a typical combustion chamber for a gas turbine the fluid mechanics are detailed with recirculation zones and injector points throughout the chamber. Numerical modeling of this type of combustion is challenging because of the interaction between the chemistry and turbulence.

The burner used in the experiment can be seen in fig. 5.2. The burner consists of a brass perforated plate with a diameter of 10.2 cm and a stainless steel tube that extends above the center of the perforated plate surface with a height of 2.54 cm. The inner diameter of the jet is 2.4 mm and the outer diameter is 6.4 mm. The perforated plate has 450 holes with diameter of 1.6 mm. The holes are separated with 4.8 mm and the blockage ratio is 0.89.

5. *Experimental Apparatus*

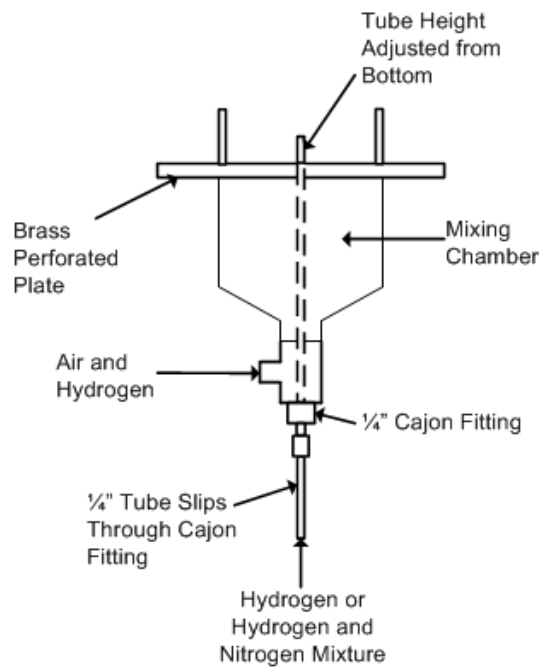
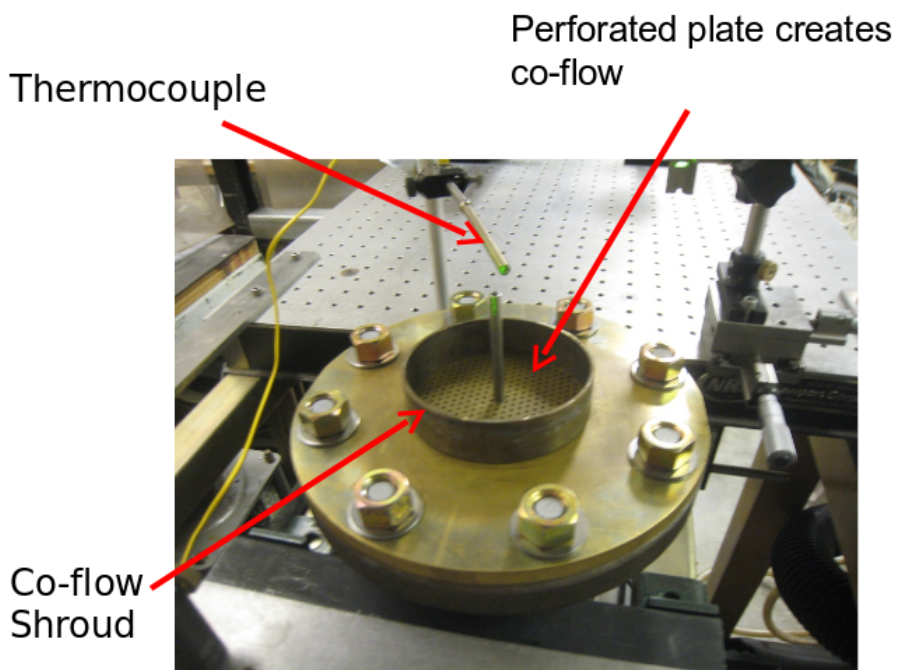


Figure 5.2.: The vitiated Co-flow Burner at Berkeley [North, 2010].

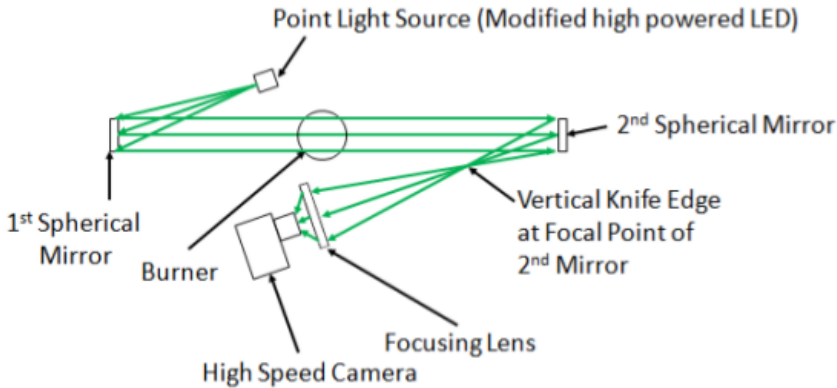


Figure 5.3.: Conceptual drawing of the schlieren imaging system [North et al., 2011].

5.2. Schlieren Imaging System

A high sensitivity Schlieren imaging system was used as part of the diagnostics for the investigation of the N_2-H_2 jet flames. Figure 5.3 shows a conceptual drawing of the Schlieren Imaging System. The system consists of a light from a high powered light emitting diode (LED), two spherical mirrors, a knife edge and a focusing lens. The system works in the following manner, the light rays from the high powered LED are made nearly parallel by the first spherical mirror. Light rays will therefore spread slowly as it propagates. This is called collimated light. The collimated light passes over the burner to the second spherical mirror which focuses the light at the location of a knife edge. The focusing lens then focuses the remaining light into the lens of a high speed camera. The knife edge allows shadows to form on the image if the light has been bent or refracted due to density gradients in the jet flame resulting from combustion. The light that is blocked by the knife edge manifests itself as shadow on the image. Thus the light that is being bent off by gradients in concentration in the combustion zone will hit the knife edge and be seen as darker or black spots on the image [North, 2010].

Schlieren imaging is used because it captures statistical information which direct imaging cannot capture because direct imaging is too time averaged

5. Experimental Apparatus



Figure 5.4.: Direct imaging of hydrogen jet flame with shutter times of 8 ms, 5 ms and 1 ms from left to right showing that direct imaging does not work [North, 2010].

for gathering statistical information [North, 2010]. The hydrogen jet flames are not bright enough to be captured by direct imaging at high speed. This is illustrated in fig. 5.4. At an exposure time of 8 ms the image is significantly time averaged. With an exposure time of 5 ms the image is blurry and with a reduction of the brightness. With an exposure time of 1 ms the image is dark and the flame barely visible. The shutter time needed to adequately capture turbulent fluctuations are much shorter than the shutter times showed in the figures. Well resolved images with a very short shutter time are possible to obtain with Schlieren imaging. Figure 5.5 shows two pictures taken by the schlieren imaging system. Here a shutter time of $156 \mu\text{s}$ is used. The liftoff heights are clearly visible in the images.

The Schlieren imaging system used in the experiments is shown in fig. 5.6. The mirrors have a diameter of 15.24 cm. The camera used has a maximum shutter speed that does not overly diminish image brightness of $25 \mu\text{s}$. This

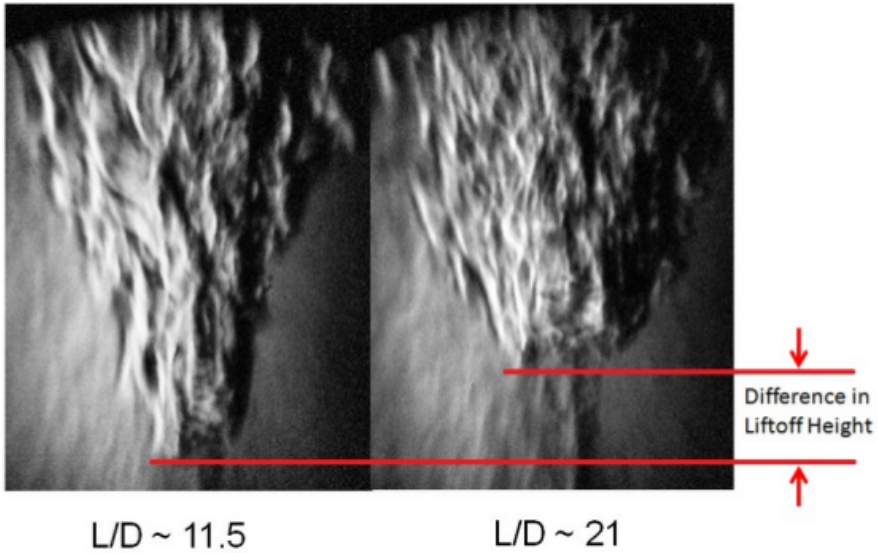


Figure 5.5.: Comparison of liftoff heights clearly made visible by the schlieren imaging system [North, 2010].

allows well resolved pictures to be obtained even with high levels of turbulence. The camera can take video of a frequency up to 1200 Hz. High speed video allows characterizations of the dynamic nature of the turbulent jet to be made [North, 2010].

5. Experimental Apparatus

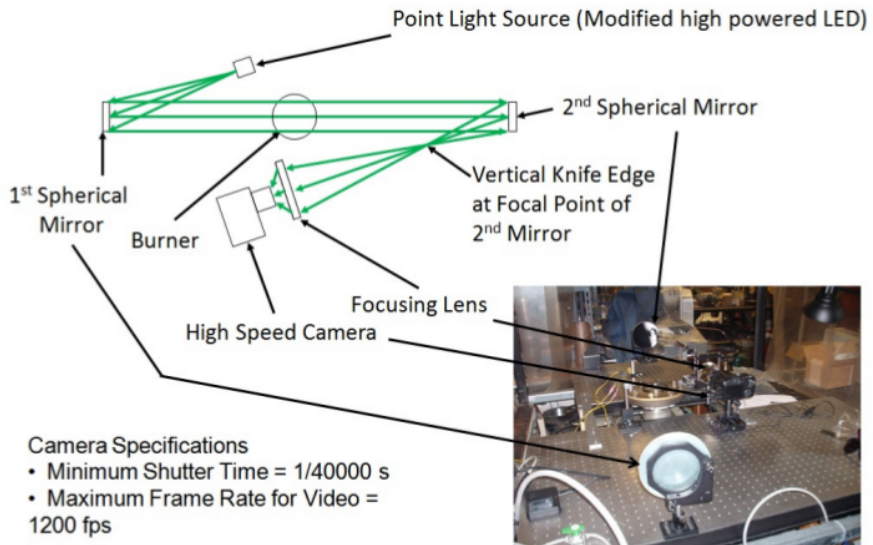


Figure 5.6.: Schlieren Imaging System used in the experiments.

5.3. Microphone Diagnostic

The recording system consists of a cardio condenser microphone which is a microphone with a heart shaped sensitivity pattern. It is designed for computer-based recordings with a USB digital output. This microphone was chosen because it has a flat frequency response meaning that the microphone is equally sensitive to all frequencies. A condenser microphone has a generally more flat frequency response than a dynamic microphone so this was chosen to assure accurate sound recordings [MediaCollege, 2011]. Furthermore, an external sound card and pre-amp is not necessary with a USB microphone. This microphone was therefore a practical choice.

The microphone was connected to a computer that applied the software All2WAV Recorder to record the signal and store the signal as a wave file. The wave file was processed numerically with MATLAB [MATLAB, 2010].

The microphone has a sampling rate of 44100 Hz. This greatly exceeds the Nyquist sampling theorem that states that the sampling rate must be greater than twice the highest-frequency component of the original signal in order to reconstruct the original waveform correctly and avoid aliasing [Wheeler and Ganji, 2004, Ch.5].

Figure 5.7 shows the experimental setup including the VCB, the Schlieren imaging system and the microphone.

5. *Experimental Apparatus*

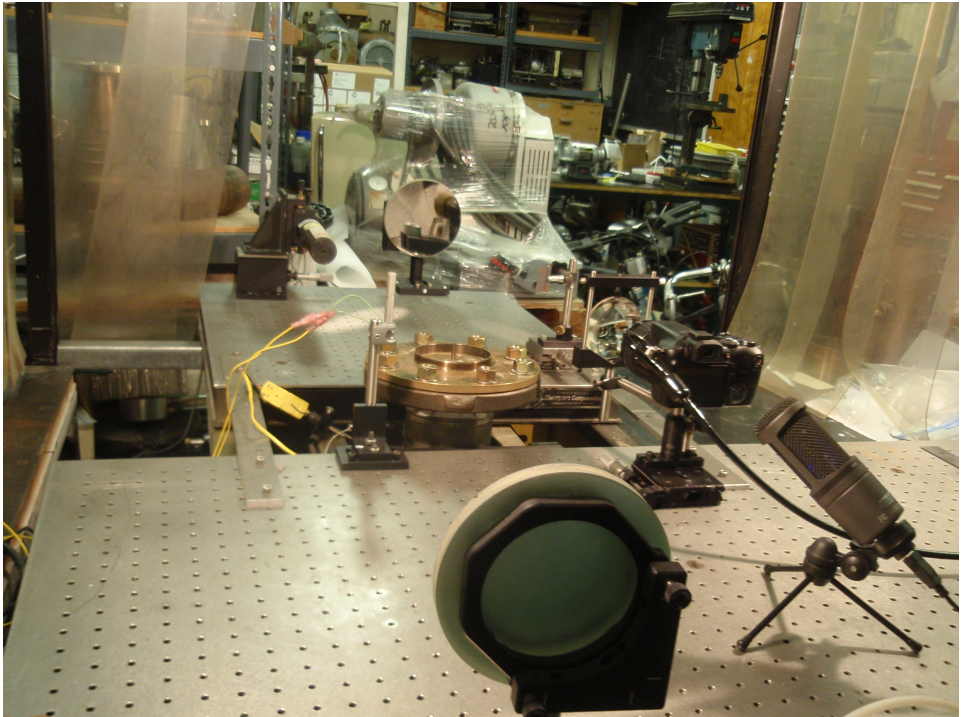


Figure 5.7.: The experimental apparatus of the Vitiated Co-flow Burner with the Schlieren imaging system and microphone.

6. Methodology

In this chapter the methodology of the experiments is described. The unsteady N₂-H₂ jet flame was investigated at atmospheric pressure as a function of jet velocity, V_{jet} , nitrogen dilution mole fraction, Y_{N_2} , and co-flow temperature (equivalence ratio, $\Phi_{co-flow}$). The unsteady regions in the stability diagrams of the N₂-H₂ jet flames found by North et al. [North et al., 2011] presented in fig. 3.2 in section 3 are the focus of the present report and were investigated in detail. It can be seen that for a co-flow equivalence ratio of 0.2 and larger, the flame is no longer attached or lifted but unsteady for all the velocities investigated. This phenomenon was investigated with high speed video by North et al. [North et al., 2011] which revealed that the flame was continuously blown out and then re-attached. It was found that the re-attachment of the flame occurred so fast that the flame speed would have to be at least 28 m/s for it to be caused by flame propagation. Therefore it was assumed that the re-attachment of the flame is a result of autoignition.

The experiments were conducted in the following manner. The jet velocity was kept constant at $V_{jet}=300, 400$ and 500 m/s. The co-flow temperature was adjusted by adjusting the co-flow equivalence ratio as the temperature increases with increasing equivalence ratio, see chapter 2.2. The co-flow equivalence ratio was increased from a value of 0.20 to 0.27. These two values were used because 0.20 is the point where the flame starts to become unsteady and at a co-flow equivalence ratio of 0.27 the flame is close to the point where it goes directly from an attached flame to blown out when the nitrogen dilution mole fraction is increased according to North et al. [North et al., 2011]. For every co-flow equivalence ratio used, the nitrogen dilution mole fraction was adjusted from the point where the flame is first unsteady until the point where the flame is completely blown out. This way a large part of the area between the stability regime boundaries in fig. 3.2 was investigated.

The case with a jet velocity of 400 m/s is the main case and was investigated for co-flow equivalence ratios of $\Phi_{co-flow}= 0.2, 0.21, 0.22, 0.23, 0.24, 0.25,$

6. Methodology

Table 6.1.: $\Phi_{co-flow}$ with the corresponding calculated temperatures.

$\Phi_{co-flow}$	Temperature [K]
0.18	754.1
0.19	782.8
0.20	811.0
0.21	838.7
0.22	866.1
0.23	893.1
0.24	919.7
0.25	945.9
0.26	971.9
0.27	997.5

0.26 and 0.27. The cases with jet velocities of 300 m/s and 500 m/s were investigated with co-flow equivalence ratios of $\Phi_{co-flow}=0.20, 0.22, 0.24, 0.25$ and 0.27. The average frequency of ignition was found for varying nitrogen dilution mole fractions for each of the cases. The average frequency of ignition will be denoted as the ignition frequency in the following.

In addition, the flames were investigated for the equivalence ratios of 0.18 and 0.19 for the three different velocities. Here the point where the flame becomes unsteady and the point where the flame is blown out were reported in order to create a complete regime diagram for the flames with the three different velocities.

The exit temperature of the jet was approximately $T_j=298$ K. The flow rate of the co-flow was held constant to 300 l/s which corresponds to a velocity of 0.65 m/s before the combustion.

According to equation 2.5 given in section 2.4 the co-flow equivalence ratio of 0.2 corresponds to a temperature of 811 K which is the temperature at which unsteady flames were produced at this geometry (jet diameter) by the previous experiment [North et al., 2011]. The temperature corresponding to a given co-flow equivalence ratio calculated from equation 2.5 can be seen in table 6.1 for the co-flow equivalence ratios used in the experiment.

The two following methods were used in the investigation of the unsteady flame:

- Acoustic recordings
- High Speed Video

These methods will be described in the following sections.

6.1. Audio Signal Analysis

The main method used for the investigation of the unsteady jet flame was acoustic recordings. A microphone was used to record the sound the flame makes when it ignites which can be characterized as a loud “popping” sound. The wave files were numerically processed in MATLAB. In order to find a fast and unambiguous method to determine the ignition frequency of the jet, several methods of signal processing were investigated. The raw audio signal was often noisy and for the cases with high frequency of ignition the sound signals were difficult to interpret. The investigation also included a large number of sound recording and it was desired to streamline the process of determining the ignition frequency. The MATLAB codes described in the following sections are given in appendix D.

Method of counting peaks

The method of counting peaks is simply to look at the time-amplitude response from the sound signals plotted as wave files in MATLAB and count the occurrences of high peaks. The normalized amplitude of the sound was plotted in MATLAB as a function of time. The raw unfiltered signal of a sound recording of a flame with $V_{jet}=400$ m/s, $\Phi_{co-flow}=0.20$ and $Y_{N_2}=0.324$ is shown in fig. 6.1. A moving average filter was applied to the sound signal. A moving average filter works as a low pass filter and is used to remove random noise while it retains the sharp response as explained in section 2.6 [Smith, 1997]. The signal after the filter has been applied can be seen in fig. 6.2. The filter has been applied with three different filter widths. The figures on the left side shows the result of applying the filter on the audio signal shown in fig. 6.1 and the figures on the right side shows the result of applying the moving average filter on the absolute value of the signal. It can be seen that the high frequency noise of the signal is increasingly removed with an increasing filter width and that the amplitude is decreasing with an increasing filter width. By applying the filter to the absolute value of the signal an increasing filter width can be used and still keep the high

6. Methodology

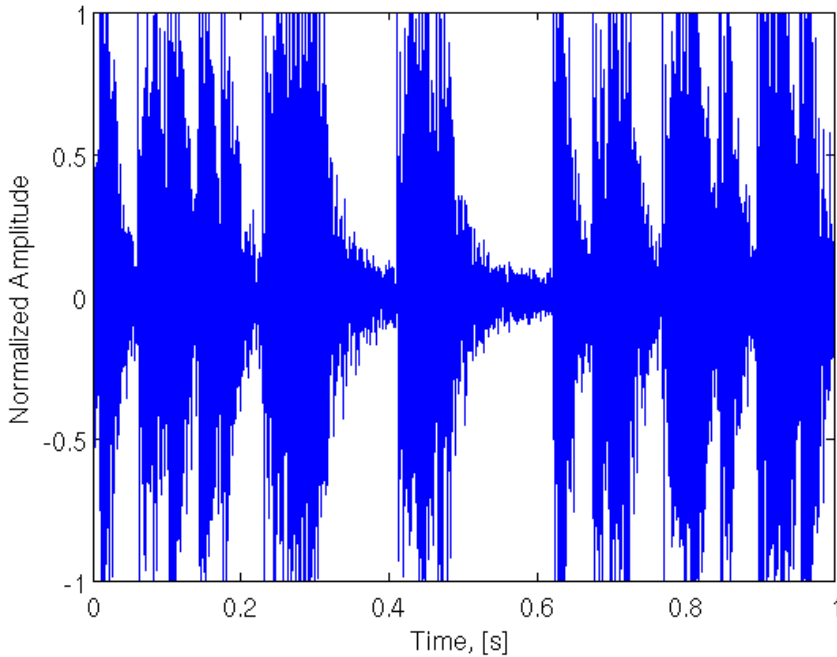
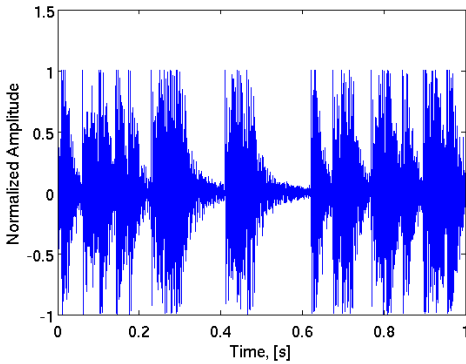


Figure 6.1.: Raw unfiltered time-amplitude response for jet flame with $V_{jet}=400$ m/s, $\Phi_{co-flow}=0.20$ and $Y_{N_2}=0.324$

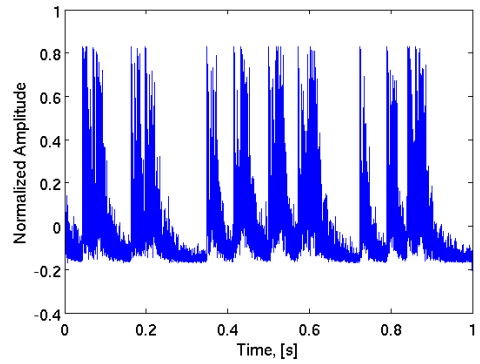
peaks. Here the signal is less noisy and the high frequency noise has been filtered away while it still has the features of the peaks. This method was time consuming and can be subjective as to what counts as a peak or not. Other methods were therefore investigated. The method of counting peaks was used in the verification of the other methods explained in the following sections.

Fast Fourier transform

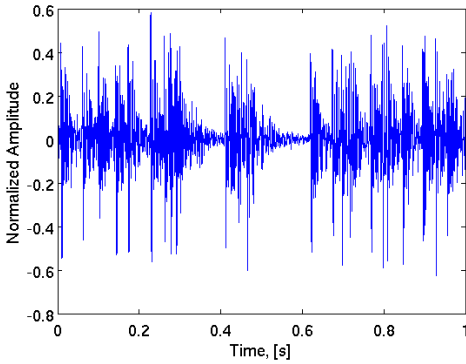
A Fast Fourier Transformation (FFT) was performed on the sound signals. Figure 6.3 shows the result from a FFT on a sound signal with $V_{jet}=400$ m/s, $\Phi_{co-flow}=0.20$ and $Y_{N_2}=0.407$. The filtered time-amplitude response for the same signal can be seen in fig. 6.4. The two different sound signals plotted in fig. 6.3 are different recordings of the same flame. The signals are



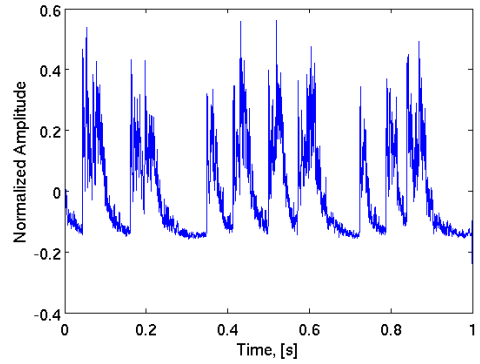
(a) Filter width of 5 points on raw signal.



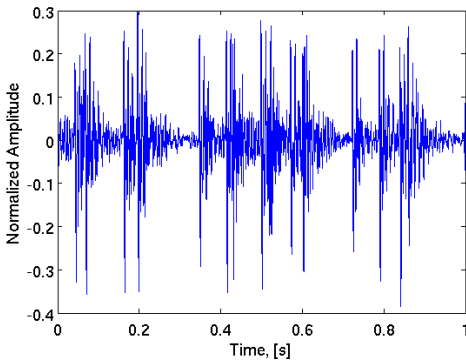
(b) Filter width of 5 points on absolute value.



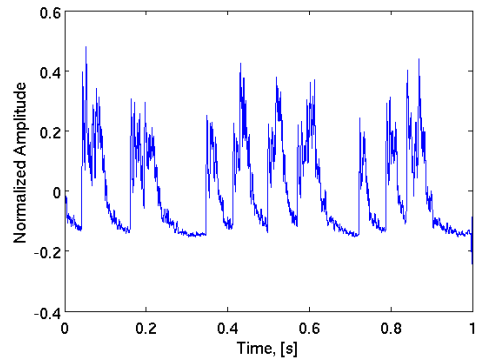
(c) Filter width of 50 points on raw signal.



(d) Filter width of 50 points on absolute value.



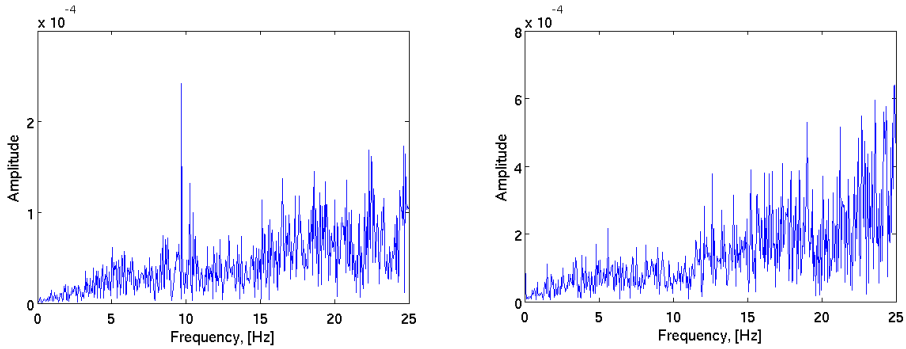
(e) Filter width of 100 points on raw signal.



(f) Filter width of 100 points on absolute value.

Figure 6.2.: Filtered time-amplitude response for flame with $V_{jet}=400$ m/s, $\Phi_{co-flow}=0.20$ and $Y_{N_2}=0.324$ with three different filter widths. Figures to the left: moving average filter on the raw audio signal. Figures to the right: moving average filter on the absolute value of the audio signal.

6. Methodology



(a) Frequency response for sound file, recording I. (b) Frequency response for sound file, recording II.

Figure 6.3.: Frequency response of sound recordings of jet flame with $V_{jet}=400\text{m/s}$ $\Phi_{co-flow}=0.20$ and $Y_{N_2}=0.407$.

plotted for a frequency range of zero to 25 Hz. In both figures several peaks are present. In fig. 6.4a the most dominant peak is the peak of around 10 Hz. This would suggest an ignition frequency of 10 Hz. In fig. 6.4b there is not one clear peak but a couple of peaks around 5 Hz and one around 12 Hz. By looking at the filtered time-amplitude response, see fig. 6.4, and counting the peaks it was found that the sound file has an ignition frequency of 2.1 Hz.

This method was eventually discarded because it did not provide a consistent result for the different sound recording of the same flame case. If the FFT had given repeatable results, validated by the counting method, then this method could have been used to rapidly finding ignition frequencies for a broad range of test conditions. One reason for why this did not work for the sound files might be the irregularity of the frequency of the ignition events. The FFT works well if the frequency is regular, but since the frequency of ignition is highly irregular with respect to time a continuous plot with absolute frequencies did not give the average frequency of the ignition events.

Integral method of the FFT

An integral method was performed on the fast Fourier transformed signal of the sound recordings. The idea was to determine the most common frequency by taking into account information from all low frequency com-

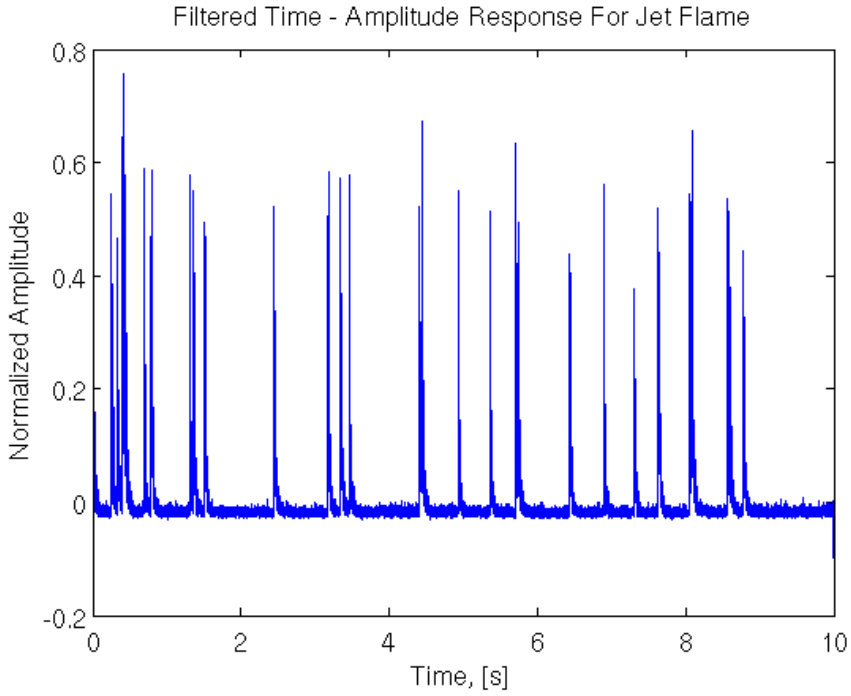


Figure 6.4.: Filtered time-amplitude response of jet flame with $V_{jet}=400$ m/s, $\Phi_{co-flow}=0.20$ and $Y_{N_2}=0.407$.

6. Methodology

ponents of the FFT through integration. The integral of the FFT from zero Hz to a predetermined maximum relevant frequency is first computed. Then, the frequency that splits this area in half is found. This frequency is theoretically the average frequency. This method did not give the correct frequency. One of the problems with this method was that it gives a different frequency for different frequency ranges chosen to integrate over. Another problem with the method was the low frequency background noise which weighted the output towards the low frequency side. A background correction was performed on the signal where the background noise was subtracted from the original sound file. This method still did not produce results consistent with the counting method, possibly because the background noise is highly variable and cannot be directly subtracted from the sound files.

The methods of Fourier transformation and integration were investigated with the objective of quickly determining the ignition frequency for any given sound signal from the unsteady jet flame. This was not obtained from the investigation. The main problem with the two methods was that they did not provide unambiguous results. It was therefore decided that the method of counting peaks was the best and most robust way of finding the ignition frequency for each sound file. The the moving average filter was applied on the absolute value of the signal. This was used to study the time-amplitude response from the signals. The number of peaks were counted and divided by the time to find the average number of ignition occurrences per second. The recorded sound signals were divided up into intervals of 0.5 to 5 seconds depending on the frequency of the signal and the peaks were counted in each interval that would make up a sound file of 20 seconds for the cases with high frequency (18-27 Hz) and 40 seconds for the sound signals with low to moderate frequencies (0-18 Hz).

In addition to counting the peaks manually, a function in MATLAB was used to count the peaks. The function counts local maximums with a given maximum peak height and minimum peak distance. Those two parameters were specified for each case after studying the sound profile since every sound profile would differ from each other with respect to amplitude and frequencies.

6.2. Video Analysis

High speed videos of 18 seconds with a frequency of 600 frames per second were taken of all the flames. The videos were studied and the number of times the flame would appear to have blown out and re-ignited was reported and divided by the time. The videos were studied in between 20 to 60 times slower than real time. This method served as a verification for the method using the acoustic recordings.

7. Results and Discussion

In this chapter the results from the experiments are described and discussed. First a comparison with previous experimental results is given. Then a characterization of the unsteady flame is provided. The results of the investigation of the ignition frequency of the unsteady flame is then given for the audio recordings and the videos. The results from these two methods are compared. Finally an uncertainty analysis is given.

7.1. Comparison with Previous Experiment

The results from the present study are compared with the results obtained by North et al. [North et al., 2011] presented in section 3 and in fig. 3.2. The stability diagram was plotted with the values obtained from the present study in order to verify that they coincide. The present study has a higher resolution of point with respect to the co-flow equivalence ratio for each of the selected jet velocities and also goes to higher nitrogen dilution mole fractions for the high velocity case ($V_{jet} = 500$ m/s).

Figure 7.1 shows the stability diagrams resulted from the present study. The plots show the existence of the four different flame regimes as found by North et al., attached, lifted, unsteady and blown out. The flames are attached for low nitrogen dilution mole fractions. By increasing the nitrogen dilution mole fraction to a value of 0.25 the flame with a velocity of 300 m/s becomes unsteady at a co-flow equivalence ratio of 0.18 and a nitrogen dilution mole fraction of 0.245. The jet flame with a velocity of 400 m/s becomes unsteady for a co-flow equivalence ratio of 0.18 and a nitrogen dilution mole fraction of 0.2. The flame with a jet velocity of 500 m/s becomes unsteady for $\Phi_{co-flow}=0.19$ and $Y_{N_2}=0.18$. For all the three cases of different velocities the flame is stable for increasing values of nitrogen dilution mole fractions for increasing co-flow equivalence ratios. These results corresponds reasonably well with the results from North et al. [North et al., 2011].

7. Results and Discussion

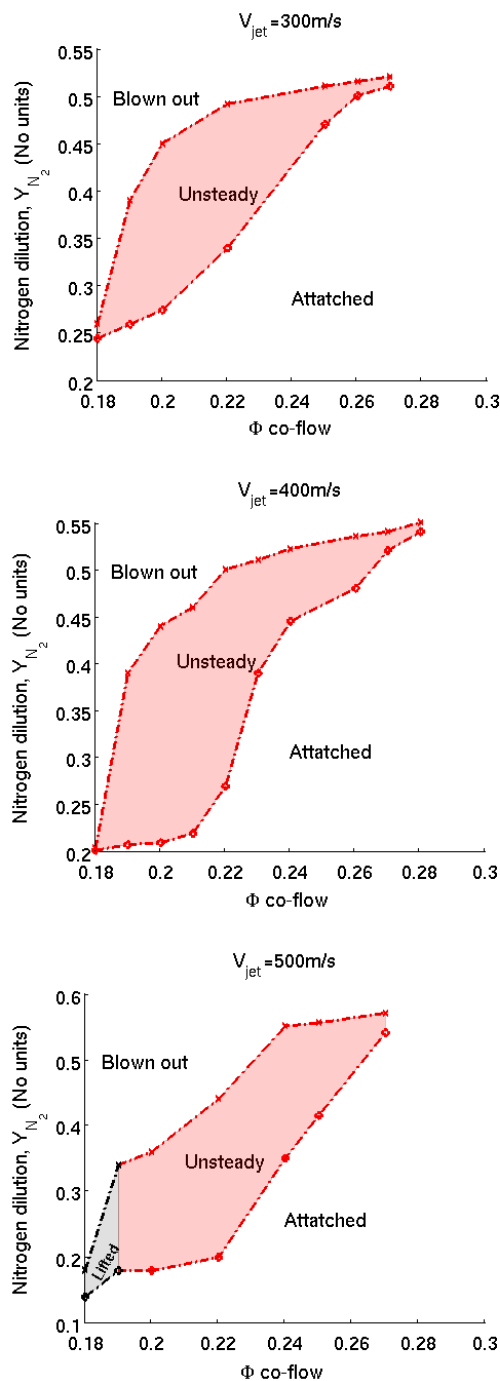


Figure 7.1.: Stability diagrams for $V_{jet}=300 \text{ m/s}$, $V_{jet}=400 \text{ m/s}$ and $V_{jet}=500 \text{ m/s}$. Four different stability regimes can be seen: attached, lifted, unsteady and blown out.

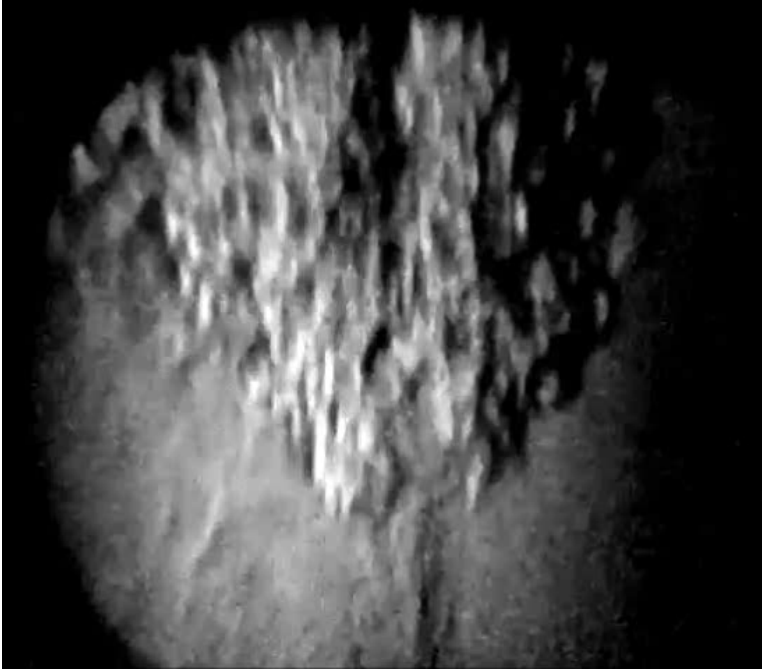


Figure 7.2.: Schlieren image of lifted N_2-H_2 jet flame in a vitiated co-flow.

7.2. Characterization of the Unsteady Flame

Turbulent flames, including the flames considered in the present work, are complex three dimensional objects that change in time because of the effects of extinction and re-ignition and due to the unstable nature of the flow. Figure 7.2 shows a picture of the Schlieren imaging of a typical lifted N_2-H_2 jet flame. The flame is clearly visible and is manifested as dark contours where the turbulent structures of the flame can be seen. The flame is lifted and the unburned N_2-H_2 gas can be seen as less dark contours.

Figure 7.3 shows a series of pictures from the Schlieren imaging of the ignition event of an unsteady flame. The ignition event occurs within 6.7 ms. Figure 7.3a shows a picture when the flame is blown out. In fig. 7.3b the flame is re-attaching. This picture is taken 3.3 ms after the first picture. The flame has the shape of a martini glass. In fig. 7.3c the flame has the shape of a normal jet flame. These pictures give an illustration of how fast the ignition occurs and what it looks like.

7. Results and Discussion

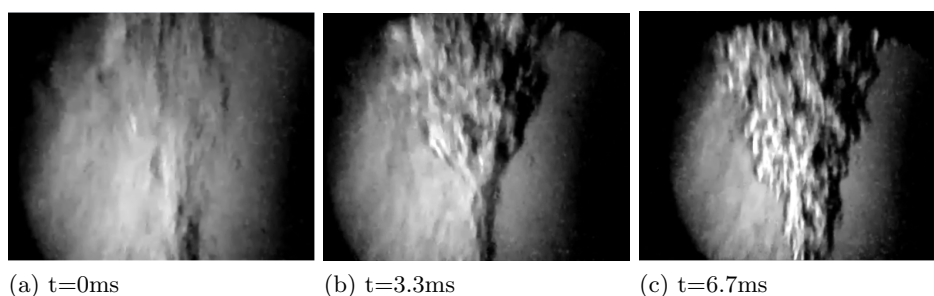


Figure 7.3.: Schlieren images of ignition event, 7.3a: Flame is blown out, 7.3b: Flame re-ignites, 7.3c: Fully ignited lifted jet flame.

Figure 7.4 shows a plot from an audio recording of one such ignition event. At first the flame is blown out and the sound signal is low. After about 0.4 seconds it ignites. The high peak shows the ignition event capturing the high sound the flame makes when it ignites. The sharp peak indicates autoignition. Then after approximately 52 μs the flame is blown out again. The ignition occurs within 3.8 μs according to fig. 7.4. This is the ignition time.

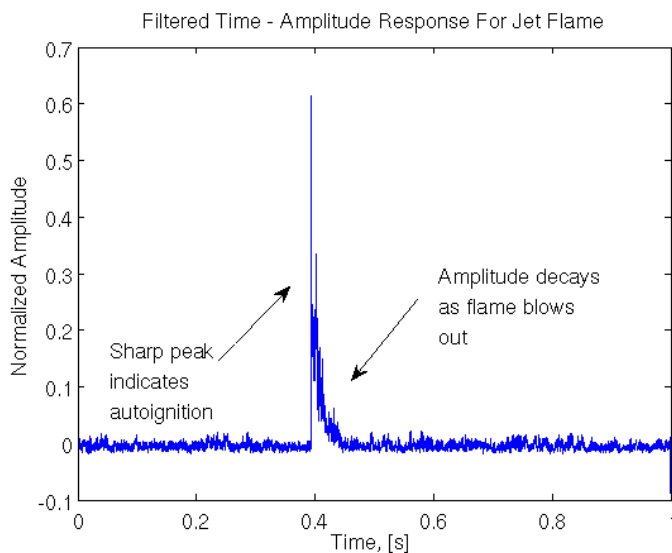


Figure 7.4.: Audio signal of one ignition event for $\text{N}_2\text{-H}_2$ jet flame with $V_{jet}=300\text{ m/s}$, $\Phi_{co-flow}=0.20$ and $Y_{\text{N}_2}=0.432$.

7.3. Frequency of the Ignition Event

The frequency of the ignition-blowout of the unsteady flames changes with altering nitrogen dilution mole fraction and co-flow equivalence ratio for the different velocities. At lower nitrogen dilution mole fractions the unsteady flame alternates between a state of an unsteady lifted flame and blowout. For the unsteady lifted flame, the liftoff height is fluctuating. When the flame blows out, re-ignition is characterized by a rapid autoigniting event. The sound signal is noisy with peaks of low frequency (0.5-5 peaks per second).

By increasing the nitrogen dilution mole fraction the ignition frequency becomes higher and the magnitude of the peaks becomes larger. At low nitrogen dilution mole fractions the frequency of ignition is only a few low peaks per second whereas as the nitrogen dilution is increased the peaks are so close that they are hard to distinguish from one another. When increasing the nitrogen dilution mole fraction further the sound signal becomes clearer, less noisy and the peaks more distinct. In this region it is easy to find the ignition frequency because the each peak is clearly distinguished from the other.

Figure 7.5 to 7.7 show the audio signals of three different conditions. Figure 7.5 is of the first type described above. The signal is noisy with intermittent peaks. This sound signal was found to have an average of 2.8 ignitions per second over 40 seconds. Figure 7.6 shows a case with high frequency. The sound signal is divided into parts of one second. This figure shows one case where it was difficult to determine the ignition frequency of the flame. The ignition frequency for this case was found to be 25.4 Hz. This is one of the highest frequencies documented in the present work. Figure 7.7 shows a case where the flame is close to blown out. Here the peaks can easily be distinguished. The ignition frequency for this case was found to be 0.8 Hz over 40 seconds.

7. Results and Discussion

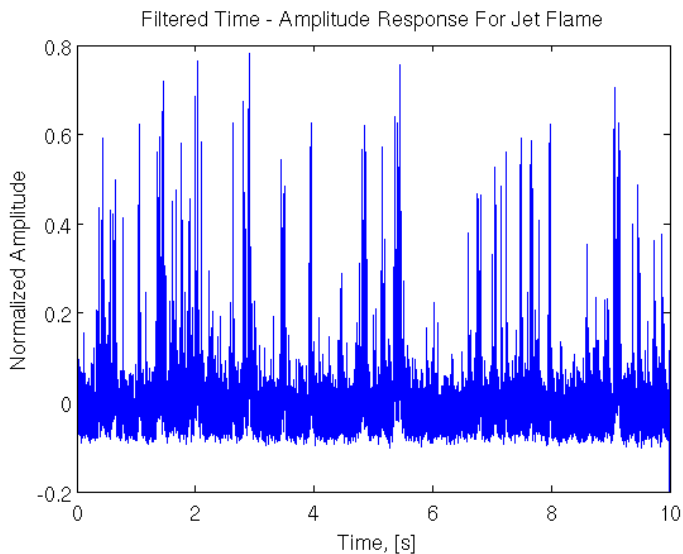


Figure 7.5.: Audio signal for N_2 - H_2 jet flame with $V_{jet}=500$ m/s, $Y_{N_2}=0.229$ and $\Phi_{co-flow}=0.22$.

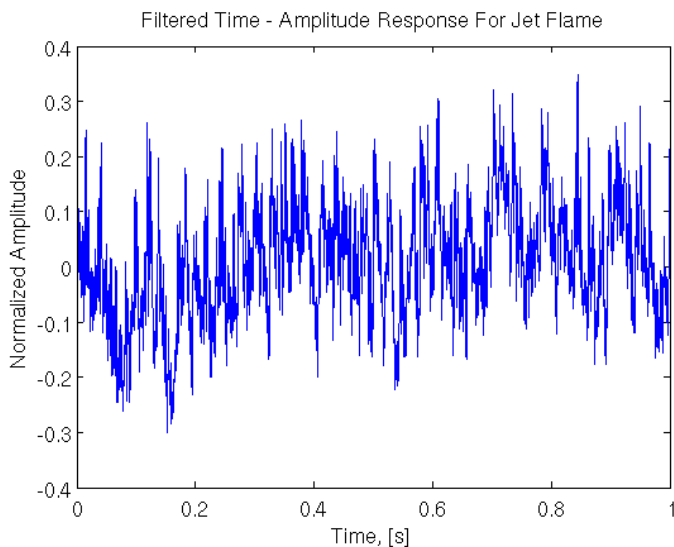


Figure 7.6.: Audio signal for N_2 - H_2 jet flame with $V_{jet}=500$ m/s, $N_{N_2}=0.294$ and $\Phi_{co-flow}=0.22$.

7.3. Frequency of the Ignition Event

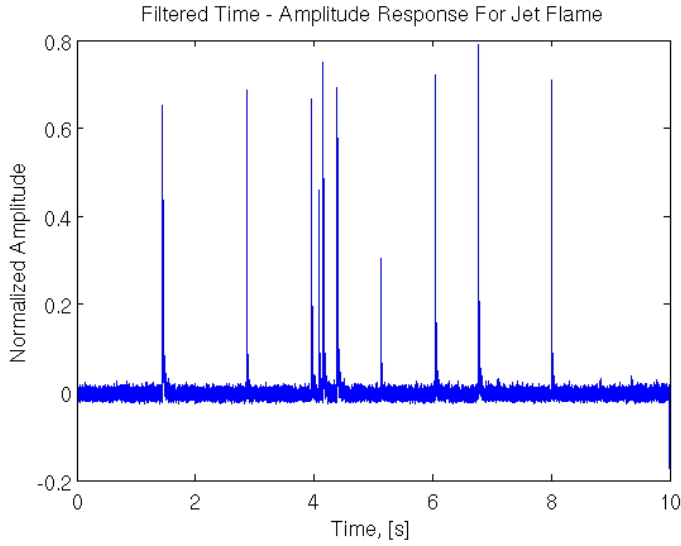


Figure 7.7.: Audio signal for N_2 - H_2 jet flame with $V_{jet}=500$ m/s, $Y_{N_2}=0.431$ and $\Phi_{co-flow}=0.22$.

7.3.1. Results from the Audio Signal Analysis

The results for the ignition frequency from the audio recordings can be seen in fig. 7.8 to 7.10 for the three different jet velocities. A complete table of all the results can be seen in appendix A. It can be seen that the ignition frequency follows the same trend for all the cases with respect to nitrogen dilution mole fraction in the jet. The ignition frequency first increases with increasing nitrogen dilution mole fraction and after reaching a maximum the frequency decreases with further increasing of the nitrogen content in the jet. This is illustrated with one single plot in fig. 7.11. On the left side of the maximum frequency the flame is oscillating between a lifted flame with fluctuating liftoff height and blown out and the ignition frequency is increasing with increasing nitrogen dilution mole fraction. An ignition frequency of zero means that the flame is lifted and no blowout occurs. At the right side of the maximum frequency the flame is oscillating between blown out and lifted flame and the ignition frequency is decreasing with increasing nitrogen dilution mole fraction. An ignition frequency of zero on this side of the maximum frequency means that the flame is completely blown out, no re-ignitions occur.

7. Results and Discussion

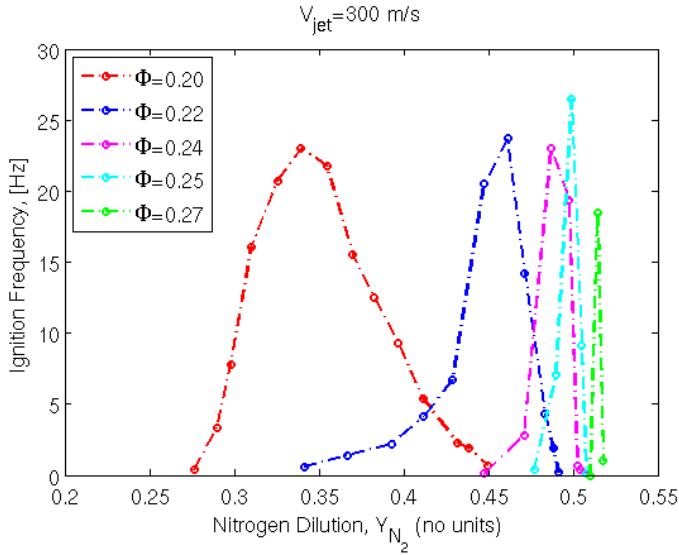


Figure 7.8.: Ignition frequency as a function of Y_{N_2} for $V_{jet}=300 \text{ m/s}$ from audio recordings.

The trend of the plots with lower co-flow temperature are better defined than the trend for the cases with higher co-flow temperatures. For higher co-flow temperatures the flame becomes unsteady at higher nitrogen dilution mole fractions. The curve is steeper and fewer data points are available since the flame is unsteady over a smaller range of nitrogen dilution mole fractions.

The nitrogen dilution affects the flame in two ways, by increasing the momentum of the jet and by slowing down the chemistry. The ignition frequency first increases with increasing nitrogen dilution mole fraction because the turbulent flame speed decreases with increasing nitrogen dilution mole fraction which encourages blowout. Blowout occurs because the turbulent flame speed is not high enough to maintain a lifted or attached flame. When the content of nitrogen in the jet is increased the flame speed is reduced and the momentum of the mixture is increased due to the high density of nitrogen compared with hydrogen. A lifted and blown out flame therefore becomes obtainable. When the nitrogen content is increased to the point where the flame becomes unsteady, the flame occasionally blows out. The hot surrounding environment caused by the vitiated co-flow is at this point close to or higher than the temperature where autoignition of hydrogen is possible at atmospheric pressure. This makes it possible for the flame to

7.3. Frequency of the Ignition Event

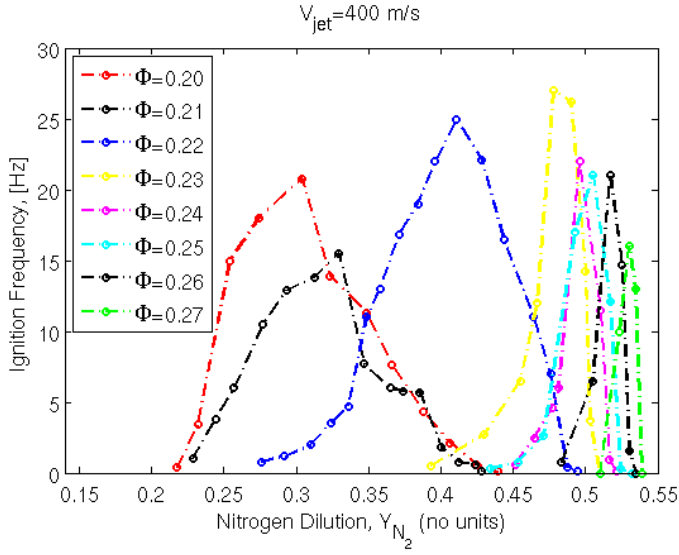


Figure 7.9.: Ignition frequency as a function of Y_{N_2} for $V_{jet}=400 \text{ m/s}$ from audio recordings.

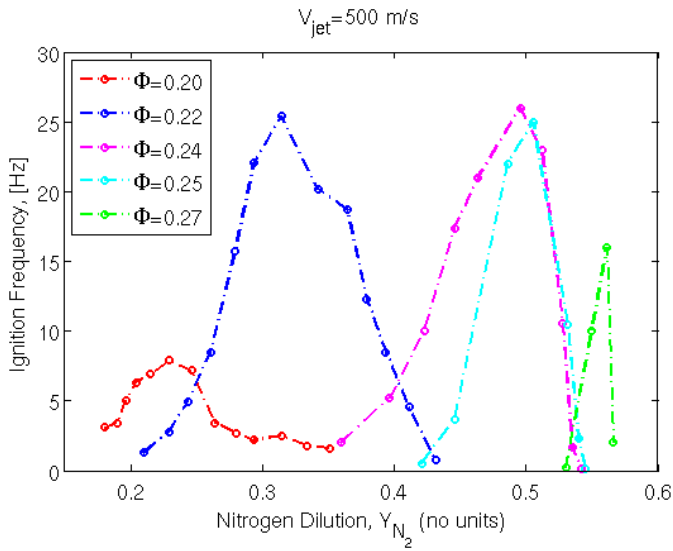


Figure 7.10.: Ignition frequency as a function of Y_{N_2} for $V_{jet}=500 \text{ m/s}$ from audio recordings.

7. Results and Discussion

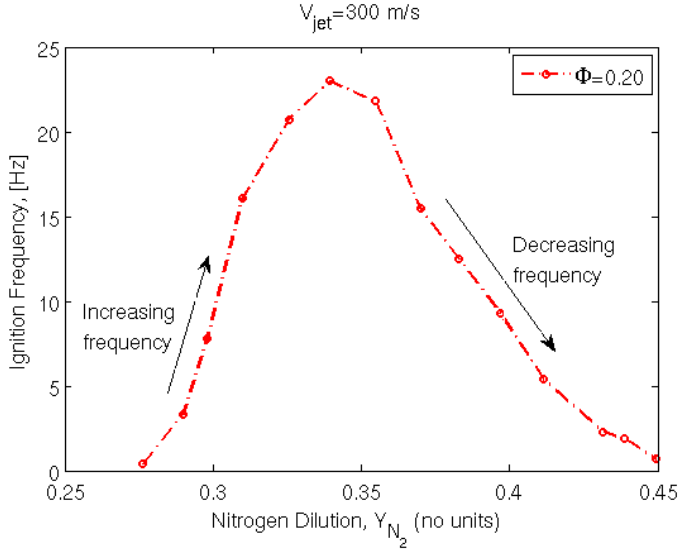


Figure 7.11.: Ignition frequency as a function of Y_{N_2} for $V_{jet}=300 \text{ m/s}$ and $\Phi_{co-flow}=0.20$ from audio recordings.

reattach by autoignition after the flame has been blown out.

When the flame reaches the point where it first becomes unsteady it rapidly re-attaches. It alternates between being a lifted flame with fluctuating liftoff height and rapid blow out-re-ignition events. The lifted flame with fluctuating liftoff height also emit some sound which leads to the noisy sound signal.

The frequency increases with increasing nitrogen dilution mole fraction because the flame speed decreases which encourages blow out more frequently, as mentioned above. The nitrogen content in the jet also affects the autoignition temperature of the mixture. Since nitrogen is essentially an inert gas the autoignition temperature decreases with increasing nitrogen content. This might be an explanation for why the ignition frequency starts to decay after reaching a maximum. The flame is at a point where the increasing autoignition temperature delays ignition and at the same time the low flame speed makes the blowout occur faster. This results in the acoustic characteristic with a clear sound profile with clearly distinguishable peaks.

The flames reaches the point of an unsteady flame for higher nitrogen content as the co-flow temperature is increased. One reason for this might be that

7.3. Frequency of the Ignition Event

the temperature affects the flame speed. Increasing temperature leads to an increasing flame speed. When the surrounding temperature of the flame increases the higher flame speed necessitates a higher nitrogen dilution mole fraction to reduce the flame speed such that a lifted and blown out flame can be achieved.

The fact that the flame is completely blown out for a higher nitrogen dilution mole fraction for increasing co-flow equivalence ratios is not surprising given the higher temperature and thus higher statistical likelihood of autoignition. The ignition delay time is strongly reduced by increasing the temperature. A higher nitrogen dilution mole fraction is therefore needed to decrease the autoignition temperature below the co-flow temperature to prevent autoignition.

Figure 7.12 to 7.16 show the results plotted for the same $\Phi_{co-flow}$ of 0.20, 0.22, 0.24, 0.25 and 0.27 for the three different velocities. All the plots given in the figures correspond reasonably well with each other with respect to maximum ignition frequency and shape with one exception. The case with a velocity of 500 m/s and a co-flow equivalence ratio of 0.20, see fig. 7.12, has a much lower maximum frequency than the rest of the plots with the same co-flow equivalence ratio. This can also be seen in fig. 7.10. The maximum frequency of this case is of 7.9 which is low compared to the other velocities with the same co-flow equivalence ratios that has maximum amplitudes of 20.8 and 23.0.

For the two low co-flow equivalence ratios of 0.20 and 0.22 the plots in fig. 7.12 and 7.13 show a clear trend. As the jet velocity is reduced, more nitrogen dilution is needed to produce the same frequencies of ignition. When the co-flow equivalence ratio is increased to 0.24 and 0.25 as seen in fig. 7.14 and 7.15 the case with a velocity of 500 m/s has a much wider range of nitrogen dilution mole fractions where the flame is unsteady than the two lower velocities. The two lower velocity cases show almost the same dependency on nitrogen dilution mole fraction for a co-flow equivalence ratio of 0.24 while for an equivalence ratio of 0.25 the flame with a velocity of 400 m/s has a much broader region where the flame is unsteady than the flame with a jet velocity of 300 m/s. For a high co-flow equivalence ratio of 0.27 more nitrogen dilution is needed to produce the same frequency of ignition as the jet velocity is increased. The nitrogen dilution range over which the flame is unsteady is increasing with increasing velocity.

The behavior of the jet flame as a function of the velocity observed in fig. 7.12 to 7.16 can be explained as follows. An increase in the velocity leads to

7. Results and Discussion

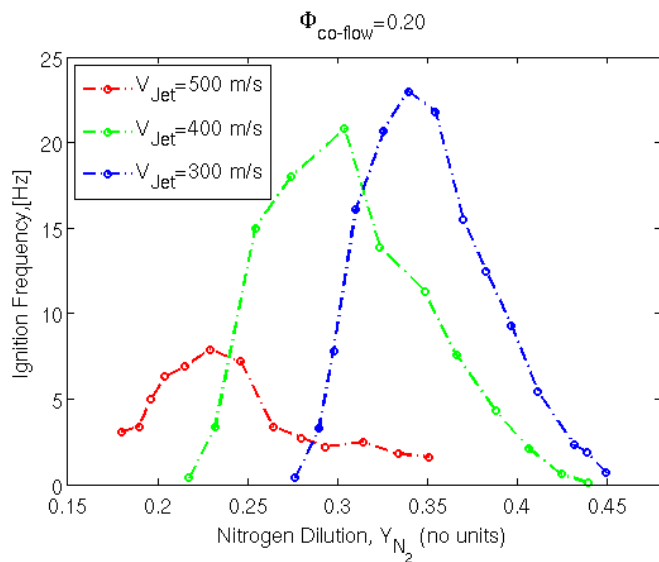


Figure 7.12.: Ignition frequency as a function of Y_{N_2} for $\Phi_{co-flow}=0.20$ from audio recordings.

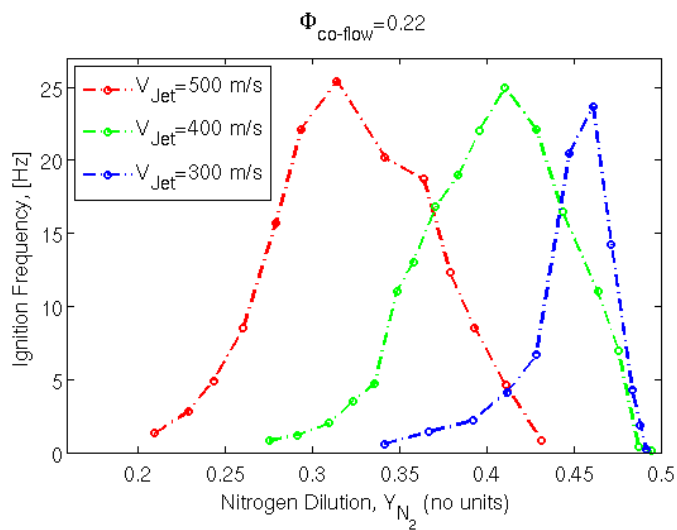


Figure 7.13.: Ignition frequency as a function of Y_{N_2} for $\Phi_{co-flow}=0.22$ from audio recordings.

7.3. Frequency of the Ignition Event

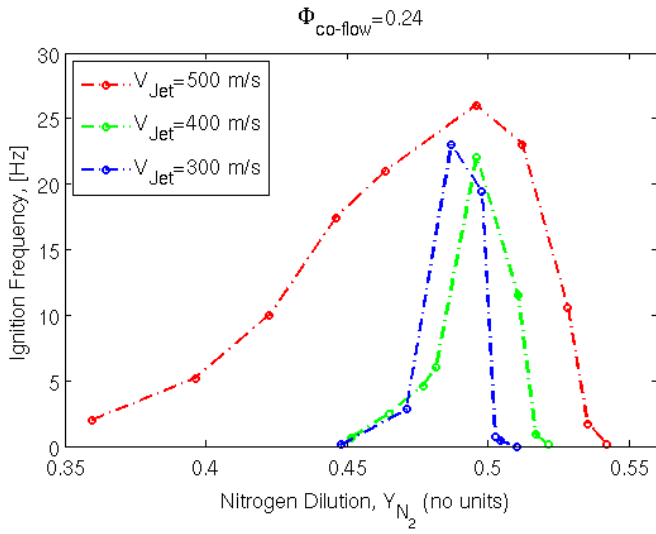


Figure 7.14.: Ignition frequency as a function of Y_{N_2} for $\Phi_{co-flow}=0.24$ from audio recordings.

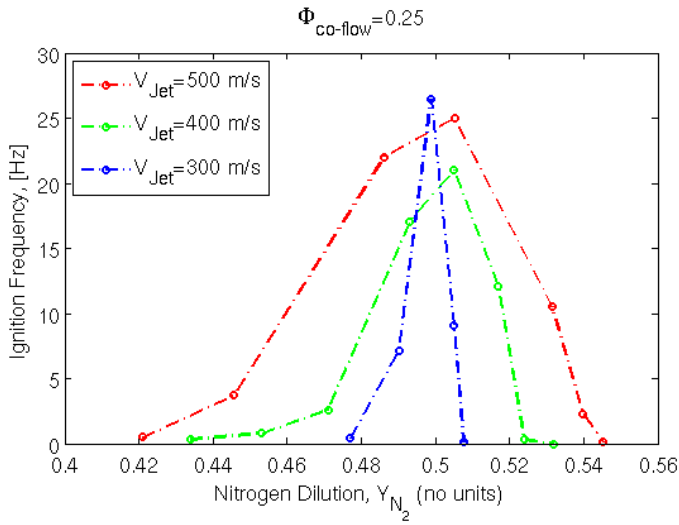


Figure 7.15.: Ignition frequency as a function of Y_{N_2} for $\Phi_{co-flow}=0.25$ from audio recordings.

7. Results and Discussion

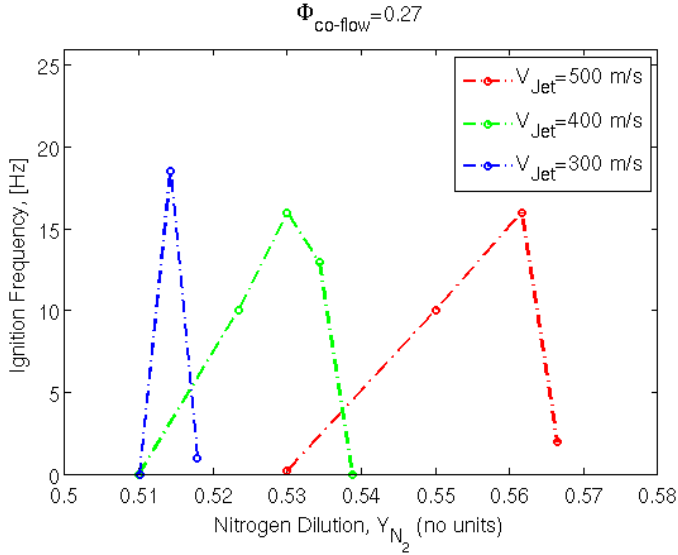


Figure 7.16.: Ignition frequency as a function of Y_{N_2} for $\Phi_{co-flow}=0.27$ from audio recordings.

an increase in the momentum of the jet which leads to a higher turbulence intensity and a higher scalar dissipation rate. Increasing scalar dissipation rate leads to increasing mixing. An increase in jet velocity also increases the total amount of hydrogen present in the flame. The increase of the momentum of the jet is the explanation for why a lifted, unsteady and blown out flame will be obtained for decreasing nitrogen dilution mole fractions for increasing jet velocities. This was seen for the equivalence ratios of 0.20 and 0.22 where the flame with increasing velocity reaches both an unsteady condition and blowout for decreasing nitrogen dilution. With co-flow equivalence ratios of 0.24, 0.25 and 0.27 the range of nitrogen dilution for which a flame is unsteady is increasing with increasing velocity. The high velocity case becomes unsteady at lower nitrogen dilution mole fraction but blows out at higher nitrogen dilution mole fractions. The reason for why the case with higher velocity blows out for higher nitrogen dilution mole fractions can be explained by the increase in mixing caused by the increasing turbulence intensity. Localized turbulent mixing can transport radicals from a location where the concentrations of radicals is large to a location where the temperature is high enough for reactions to occur which might lead to ignition. This combined with the higher ignitability of the jet as a result of increasing amounts of hydrogen in the jet leads to the increasing range of

7.3. *Frequency of the Ignition Event*

unsteady flames with increasing velocity.

7.3.2. Results from the Video Analysis

In this section the results from the high speed Schlieren imaging videos are presented. The results are given for low equivalence ratios of 0.20 to 0.22. The reason for the limited results from the high speed videos is that with the Schlieren imaging system it becomes increasingly difficult to distinguish between the jet flame and the co-flow as the co-flow temperature increases and thus the density gradients decrease. The increase in density gradients leads to an increase in the gradient of the index of refraction. The Schlieren imaging gave better videos for flames with an increasing velocity because the increasing velocity increases the momentum of the jet and thereby the density gradients between the jet and the co-flow. This is the reason for why the high speed videos only gave results for a co-flow equivalence ratio of 0.20 for the case with a jet velocity of 300 m/s and results for up to an equivalence ratio of 0.22 for jet velocities of 400 m/s and 500 m/s.

Figure 7.17 to 7.19 show the results from the videos for the flames with the three different velocities. The results are also given in tables in appendix A.2. The results from the high speed videos show the same trends as the results from the audio recordings. The average frequency increases with increasing nitrogen dilution mole fraction until it reaches its maximum and from there it decreases with increasing nitrogen dilution mole fraction. From fig. 7.18 and 7.19 it can be seen that the results from the high speed videos show the same trend as the results from the audio recordings with respect to how the ignition frequency is influenced by the co-flow temperature. An increase in co-flow temperature leads to higher nitrogen dilution mole fraction to produce the same ignition frequency.

7.3. Frequency of the Ignition Event

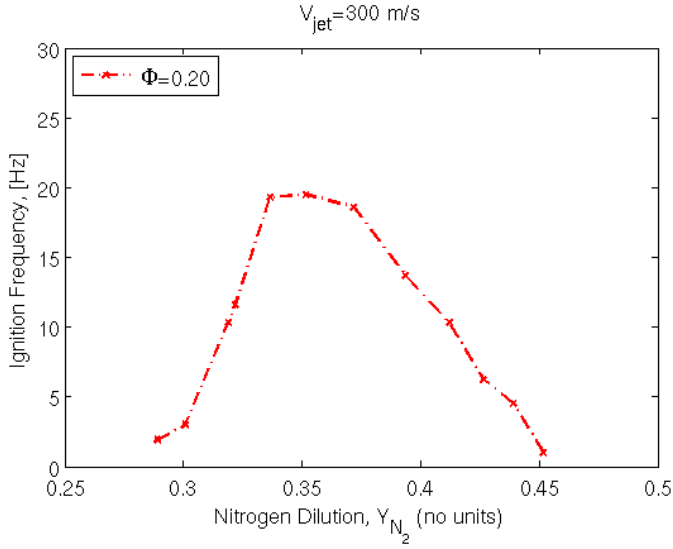


Figure 7.17.: Ignition frequency as a function of Y_{N_2} for $V_{jet}=300$ m/s from high speed video

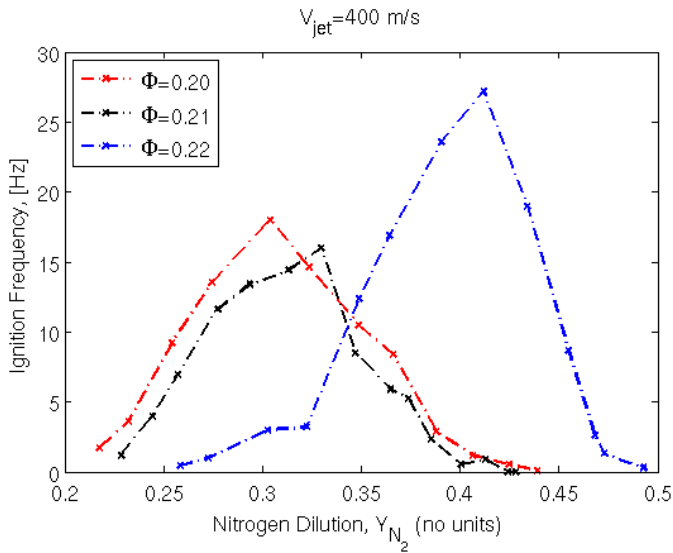


Figure 7.18.: Ignition frequency as a function of Y_{N_2} for $V_{jet}=400$ m/s from high speed video

7. Results and Discussion

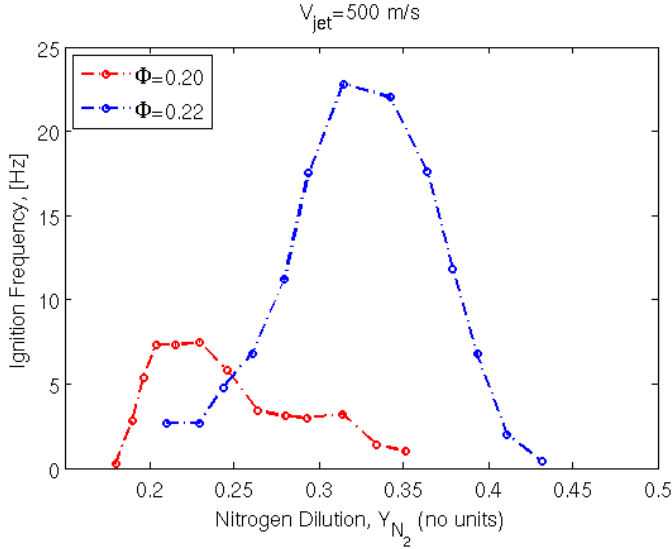


Figure 7.19.: Ignition frequency as a function of Y_{N_2} for $V_{jet}=500$ m/s from high speed video

7.4. Comparison between Audio and Video Results

In this section the results from the audio recordings and the high speed videos are compared. The results can be seen in fig. 7.20 to 7.22.

The results from the two different methods follow each other reasonably well for all the three velocities. The case with a jet velocity of 300 m/s the results deviates from each other more than from the two other velocities. The reason for this might be that the video recordings for this case were made separately from the audio recordings and in the process of recreating the exact same case there might occur some deviation in co-flow equivalence ratio which might have lead to the deviation in the results. The uncertainty of the results are highly sensitive to changes in the co-flow temperature, see section 7.5. This is also the case for $V_{jet} = 400$ m/s and $\Phi_{co-flow}$. For this case the results follow each other well. The results for $V_{jet}=500$ m/s correspond well with the results from the audio recordings for both the cases which includes the case of $\Phi = 0.20$ which deviates from the other cases with respect to the maximum ignition frequency.

In general the results from the two methods coincide sufficiently well and the results from the high speed videos gives a good verification of the method

7.4. Comparison between Audio and Video Results

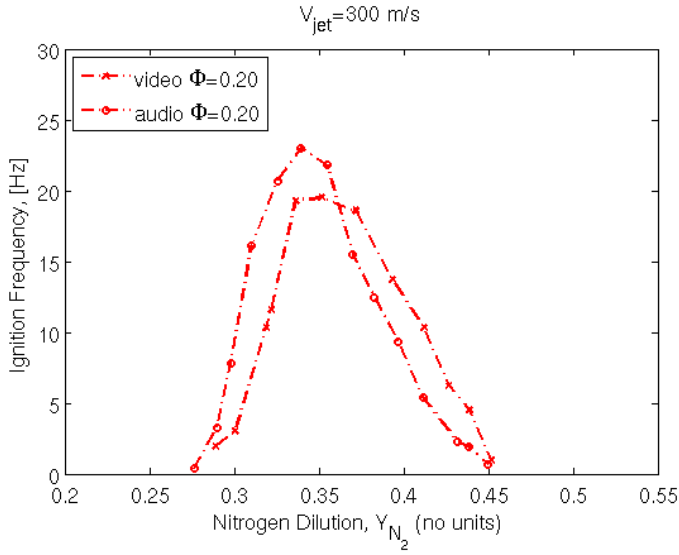


Figure 7.20.: Comparison of results from audio recordings and high speed video. Ignition frequency as a function of Y_{N_2} for $V_{jet}=300$ m/s.

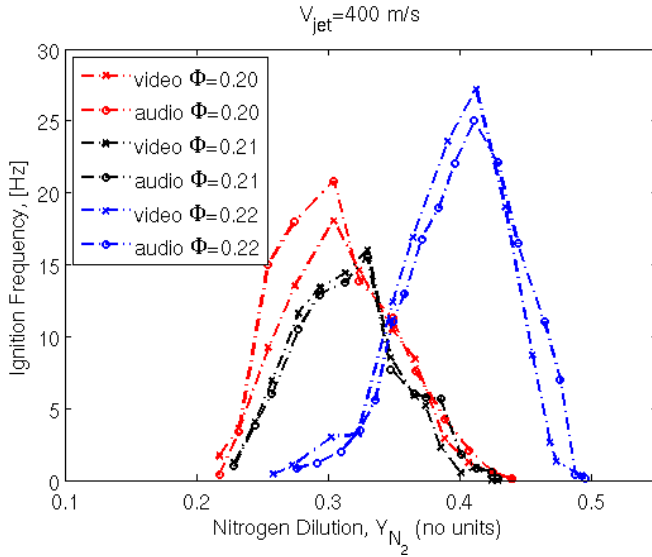


Figure 7.21.: Comparison of results from audio recordings and high speed video. Ignition frequency as a function of Y_{N_2} for $V_{jet}=400$ m/s.

7. Results and Discussion

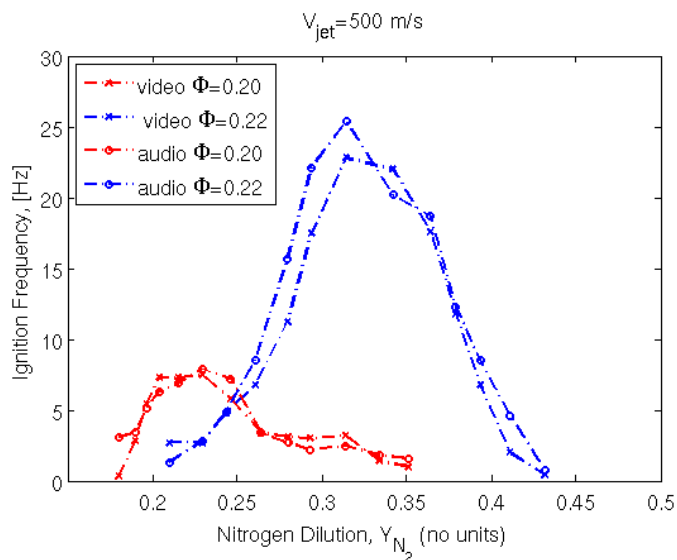


Figure 7.22.: Comparison of results from audio recordings and high speed video. Ignition frequency as a function of Y_{N_2} for $V_{jet}=500$ m/s.

used for the audio recordings. The good agreement serves as verification of the method of counting peaks. The video method could be used as well but is more time consuming and more limited regarding the equivalence ratio ranges that can be investigated. This work gives confidence that the audio method can be used as a stand alone method for measuring the ignition frequency at the higher co-flow equivalence ratios.

7.5. Uncertainty Analysis

An uncertainty analysis was performed on a selection of the measurements with the objective of giving a quantification of the maximum uncertainty of the results. All the estimates were made to the same confidence interval of 95%. The uncertainty analysis is divided into an analysis of the random and the systematic uncertainty. These two uncertainties are then combined to a total uncertainty.

7.5.1. Uncertainty of the Audio Recordings

Random Uncertainty

The random uncertainty of the results from the audio recordings was found for an array of selected measurements. The t-distribution introduced in section 2.5 was used in the estimate of the random uncertainty. The two following uncertainties contribute to the total random uncertainty:

- Time step uncertainty: Uncertainty resulting from the fact that the sound bites were recorded for a finite time interval.
- Counting uncertainty: Uncertainty from ambiguities regarding what counts as a peak resulting in several different frequencies for the same sound recording counted several times.

First an analysis of the time step uncertainty was made. As mentioned previously the frequency of the ignition-blowout events is not uniform with respect to time and longer recordings would result in a more accurate frequency. It was therefore decided to find the time length that would give sufficiently accurate results. This was done by the following procedure: The average frequency was found for two different cases, one high frequency case and one low frequency case, to represent the outer boundaries. The average frequencies were found for five different samples of two seconds, 10 seconds, 20 seconds and 40 seconds to see how the uncertainty changes with the length of the time steps. The two cases used for the analysis were a jet velocity of 300 m/s, co-flow equivalence ratio of 0.22 and nitrogen dilution mole fractions of 0.461 and 0.488. The value of t from the t-distribution with $n = 5$ is 2.776 [Wheeler and Ganji, 2004].

Table 7.1 shows the results from the analysis. The uncertainty decreases with increasing time step and the uncertainty is higher for the case with

7. Results and Discussion

Table 7.1.: Random time step uncertainty for the two chosen cases with $V_{jet}=300$ m/s and $\Phi_{co-flow}=0.22$.

t [s]	N ₂ dilution, Y_{N_2}	\bar{f} [Hz]	S_x	$\pm P_{\bar{x}}$	$\pm P_{\bar{x}}$ %
2	0.461	24.2	2.28	2.83	11.7
	0.488	3.6	1.94	2.42	67.2
10	0.461	22.2	0.61	0.76	3.4
	0.488	3.0	1.36	1.69	55.9
20	0.461	23.1	0.58	0.72	3.1
	0.488	3.0	0.47	1.12	37.9
40	0.461	22.1	0.26	0.32	1.5
	0.488	3.0	0.07	0.09	6.9

low frequency than the case with high frequency for all the cases. It can be seen that for a time step length of two seconds both the high and the low frequency cases gives unacceptable high uncertainties. The uncertainty of the case with low frequency is of 67.2 % of the value of the frequency. The frequency is low and a large uncertainty in this point would therefor not have a large impact on the plots shown in fig. 7.8 to 7.10. By increasing the time step length to 10 seconds the uncertainty is reduced for both the cases but it is still unacceptably high for the low frequency case. By choosing a time step of 20 s the uncertainty is acceptable for the high frequency case, but still too large for the low frequency case. It was therefore decided to use time steps of 20 s for the cases with moderate to high frequencies and 40 s for the cases with low frequency. Note, however, that the experiments with a velocity of 300 m/s were done before this analysis with time steps of 10 s and due to time restrictions the experiments were not done over again. Therefore these results are subjected to higher uncertainty for the cases with low frequency than the cases with higher velocities.

The counting uncertainty was found for the case of a velocity of 300 m/s and a co-flow equivalence ratio of 0.20. It was found by counting the same cases five times. The results can be seen in table 7.2. For the cases with low frequency the uncertainty is zero with respect to the counting of the peaks. However, for the cases with higher frequencies there is an uncertainty of the mean varying between five and ten percentage of the value.

Table 7.2.: Random counting uncertainty of $V_{jet} = 300\text{m/s}$ and $\Phi = 0.20$.

N_2 Dilution, Y_{N_2}	\bar{f} [Hz]	S_x	$\pm P_{\bar{x}}$	$\pm P_{\bar{x}}$ %
0.276	0.4	0	0	0
0.290	3.3	0.19	0.23	7.2
0.298	10.5	0.96	1.20	11.4
0.310	18.6	1.44	1.77	9.8
0.326	20.7	0.56	0.69	3.4
0.340	26.3	1.13	1.40	5.3
0.355	23.4	1.50	1.86	8.0
0.370	15.5	0.81	1.00	6.5
0.383	11.8	0.85	1.05	8.9
0.397	9.3	0.34	0.46	5.0
0.411	5.3	0.26	0.33	6.2
0.432	2.3	0	0	0
0.439	1.9	0	0	0
0.449	0.7	0	0	0

The total random uncertainty for a flame with high ignition frequency will be dominated by the counting uncertainty while the time step uncertainty will have a negligible influence. For a flame with low ignition frequency the time step uncertainty will be dominant.

Systematic Uncertainty

The systematic uncertainty was calculated by equation 2.9, presented in section 2.5, where the result, R , is the ignition frequency. The systematic uncertainty of the experiments comes from the following sources:

- Calibration errors.
- Errors in the pressure transducers.

The variables are the flow-rates of N_2 , H_2 and co-flow consisting of H_2 and air. This leads to four different terms in equation 2.9 both with respect to pressure transducers errors and calibrations errors. Equation 2.9 will therefore have eight terms in calculating the total systematic uncertainty. The calculation of the systematic uncertainty can be seen in appendix B.

7. Results and Discussion

Table 7.3.: Results from calculation of systematic uncertainty for a flame with $V_{jet} = 400$ m/s and $\Phi_{co-flow} = 0.22$.

	$Y_{N_2} = 0.371$	$Y_{N_2} = 0.464$
f [Hz]	16.8	11
w_{pt}	6.03	0.18
w_{pt} %	35.9	1.6
w_{cal}	1.31	0.04
w_{cal} %	7.8	0.4
w_R	6.17	0.18
w_R %	36.7	1.6

The calculation has been divided into the calculation of the uncertainty of the pressure transducers and the calibration to see which of these errors has the largest impact on the total systematic uncertainty. The results from the calculation can be seen in table 7.3. Here w_{pt} denotes the uncertainty in the pressure transducers and w_{cal} denotes the calibration uncertainty. w_R denotes the total systematic uncertainty.

The accuracy of the pressure transducers for the hydrogen jet flow and the air flow is 1 % of maximum value and the accuracy of the pressure transducers used for the nitrogen and co-flow hydrogen is 0.4 % of maximum. It is assumed that these accuracies are given with a confidence interval of 95 %.

The systematic uncertainty was found for two chosen data points for a flame with a velocity of 400 m/s, a co-flow equivalence ratio of 0.22 and nitrogen dilution mole fractions of 0.371 and 0.464.

The uncertainty of the pressure transducers is much larger than the uncertainty of the calibration. The systematic uncertainty is most sensitive to changes in the co-flow equivalence ratio. A slight change in equivalence ratio will result in large differences of the frequency. The sensitivity is therefore high when it comes to the co-flow equivalence ratio.

The systematic uncertainty was only found for two cases because the sensitivity with respect to the co-flow equivalence ratio was not possible to find for many cases. The two cases the systematic uncertainty was found for varies from a high uncertainty of 36.7 % to a low uncertainty of 1.60%. It is

Table 7.4.: Random, systematic and total uncertainty estimate for a flame with $V_{jet}=400$ m/s and $\Phi_{co-flow}=0.22$.

N_2 Dilution, Y_{N_2}	$\pm P_{\bar{x}}$	$\pm P_{\bar{x}}$ %	w_R	w_R %	$W_{\bar{x}}$	$W_{\bar{x}}$ %
0.371	0.68	4.1	6.17	36.7	6.23	37.1
0.464	0.78	7.1	0.18	1.6	0.80	7.3

therefor difficult to draw a conclusion about how high the typical systematic uncertainty is.

Estimate of Total Uncertainty

The total uncertainty estimate, $W_{\bar{x}}$, was found for the two cases that the systematic uncertainty was found for by the use of equation 2.10, presented in section 2.5. The two cases used were of flames with $V_{jet}=400$ m/s and $\Phi_{co-flow}=0.22$. The random uncertainty for the two cases was found by the same method as used above for random uncertainty, see appendix C.

The time step uncertainty was used for a time step of 40 s for both the cases. The results are presented in table 7.4.

By comparing the total uncertainty estimate with the random and systematic uncertainties it can be seen that for the first case the systematic uncertainty is so large that the random uncertainty can be neglected. For the second case both the two uncertainties contributes to the total uncertainty. The high uncertainty of the first case is a result of the high sensitivity of the results to the co-flow equivalence ratio.

7.5.2. Uncertainty Analysis of the High Speed Video

An uncertainty analysis was also performed on the high speed videos. The videos were 18 seconds each. The random uncertainty connected to the length of the videos is the same as the random uncertainty connected to the length of the sound files. 18 seconds will therefore result in a high uncertainty for the cases with low ignition frequency while it is considered sufficiently long for the cases with high ignition frequency. The counting uncertainty was analyzed for the videos. The same videos were counted five

7. Results and Discussion

Table 7.5.: Random uncertainty of the high speed video results for a flame with $V_{jet}=300$ m/s and $\Phi_{co-flow}=0.20$.

N_2 Dilution, Y_{N_2}	\bar{f} [Hz]	S_x	$\pm P_{\bar{x}}$	$\pm P_{\bar{x}}$ %
0.289	2.0	0.11	0.13	6.5
0.301	3.1	0.09	0.11	3.6
0.319	9.6	0.39	0.48	5.0
0.322	11.0	0.40	0.50	4.5
0.337	19.5	0.35	0.44	2.2
0.352	18.9	0.47	0.58	3.1
0.372	18.9	0.53	0.66	3.5
0.394	13.5	0.25	0.31	2.3
0.412	9.8	0.60	0.74	7.6
0.427	6.2	0.18	0.22	3.6
0.439	4.5	0.17	0.21	4.7
0.452	1.1	0.08	0.10	9.6

times for the same cases as were used for the audio files, $V_{jet}=300$ m/s and $\Phi_{co-flow}=0.20$. The results can be seen in table 7.5. Note, however, that the cases with respect to nitrogen dilution mole fraction does not completely correspond to the cases for the audio recordings. This is because the videos were taken after the audio recordings in a separate experiment.

As can be seen from table 7.5 the counting uncertainty from the high speed videos varies with values between 2.26 % to 9.61 % of the value of the mean frequency. This uncertainty is generally higher for the low frequency cases than the high frequency cases which is the opposite of the trend for the counting uncertainty for the audio recordings. The uncertainty is especially high for the flames with low ignition frequency and high nitrogen dilution mole fractions. This is probably because the Schlieren imaging system works better with low fractions of nitrogen dilution because the gradients of the concentration is then larger between the jet flame and the surrounding air.

8. Conclusion

The present experimental study of the H_2 jet flames diluted with N_2 issued into a vitiated co-flow resulted in stability diagrams similar to those obtained by North et al. [North et al., 2011] with the same stability regimes of attached, lifted, unsteady and blown out flames.

The unsteady flames were studied in detail with varying nitrogen dilution mole fraction, co-flow temperature and jet velocity by the use of audio recordings and Schlieren imaging high speed videos. The results from both the audio recordings and the Schlieren imaging suggest that the ignition of the unsteady jet flames occurs as a result of autoignition. The following trends were found for the ignition frequency of the unsteady N_2 - H_2 flames:

- The frequency increases with increasing nitrogen dilution mole fraction in the jet until a maximum frequency is reached. After reaching the maximum frequency the frequency decreases with further increase of the nitrogen dilution mole fraction.
- For increasing co-flow temperatures the flames becomes unsteady and blows out at increasing nitrogen dilution mole fractions.
- An increase in the velocity leads to unsteady and blown out flames for decreasing nitrogen dilution mole fractions for low co-flow temperatures. Higher co-flow temperatures leads to an increasing range of nitrogen dilution mole fractions over which jet flames with increasing velocities are unsteady. An increase in the velocity leads to an unsteady flame for lower nitrogen dilution mole fractions and a blown out flame for higher nitrogen dilution mole fractions at higher co-flow temperatures.

The behavior of the unsteady flame with respect to the nitrogen content in the jet is explained by two mechanisms by which the nitrogen content affects the jet flame. An increasing nitrogen content in the jet increases the momentum of the jet and slows down the chemistry which reduces the turbulent flame speed and thereby encourages liftoff and blowout. This is

8. Conclusion

the explanation for why the frequency increases by increasing the amount of nitrogen in the jet. Nitrogen dilution affects the ignition temperature of the mixture. Increasing the amount of nitrogen in the jet increases the ignition temperature of the mixture and this can explain why the ignition frequency is reduced with increasing nitrogen dilution mole fraction in the jet after the maximum frequency has been reached.

The influence of temperature on the ignition frequency of the jet is explained by the fact that the increasing temperature increases the flame speed which makes it necessary for higher nitrogen dilution mole fractions to produce the same ignition frequencies as for lower co-flow temperatures. The ignition delay times are reduced by the increase of temperature. Therefore a higher nitrogen dilution mole fraction is needed to obtain the same ignition frequencies as for lower temperature as the co-flow temperature increases.

Increasing velocity of the jet affects the jet flames in two ways. The increase of momentum of the jet leads to an increase of the turbulence intensity and thereby an increase of the mixing of the products and reactants. The total amount of hydrogen present in the jet is increased and thus the ignitability of the mixture is increased. This is the explanation for why the range of nitrogen dilution mole fractions for which the flame is unsteady increases with increasing velocity. The increase in momentum leads to a lifted and unsteady flame for lower nitrogen dilution mole fractions while an increase in the mixing and the total hydrogen content in the gas leads to higher ignitability and a higher level of nitrogen dilution mole fraction is needed to reach blowout.

These results suggests that the autoignition phenomena of the $\text{H}_2\text{-N}_2$ jet flame issued into a vitiated co-flow is controlled by both chemistry and turbulent mixing.

The main method used to study the frequency of ignition of the unsteady $\text{N}_2\text{-H}_2$ flame was the analysis of the audio recordings. This method was verified by the high speed videos which gave confidence to audio recordings as a diagnostics for investigation of unsteady jet flames.

The total uncertainty of the results is high. The random uncertainty related to the counting of the peaks is high and the sensitivity of the frequency to the co-flow equivalence ratio is high. However, the fact that the results show a clear trend for all the cases investigated and the fact that the results from the audio recordings and high speed video follow each other well gives confidence to the results.

9. Suggestions for further work

It is suggested to continue the work of signal processing in order to find a good and unambiguous way of determining the ignition frequency of an unsteady flame that is less time consuming than the method of counting the peaks. It is suggested to look into noise correction algorithms. The uncertainty of the results is high and a method that would reduce the counting uncertainty would be advantageous for the reliability of the results.

The study of the unsteady flame at atmospheric pressure is only the first step in the investigation of ignition and blowout of the N_2-H_2 flame surrounded by a vitiated co-flow. By recognizing the essential role of pressure to determine chemical pathways, experiments at elevated pressures are crucial for the understanding of hydrogen combustion at gas-turbine conditions. Experiments of the N_2-H_2 jet flame at pressures of 2-3 bar and 8 bar are currently being planned. The effect of pressure on the N_2-H_2 jet flame in a vitiated co-flow will then be investigated.

Bibliography

- [Cabra, 2003] Cabra, R. (2003). *Turbulent Jet Flames into a Vitiated Coflow*. PhD thesis, University of California, Berkeley.
- [Cabra et al., 2005] Cabra, R., Chen, J.-Y., Dibble, R. W., Karpetis, A. N., and Barlow, R. S. (2005). Lifted methane-air jet flames in a vitiated coflow. *Combustion and Flame*, 143:491–506.
- [Cabra et al., 2002] Cabra, R., Myhrvold, T., Chen, J.-Y., Dibble, R. W., Karpetis, A. N., and Barlow, R. S. (2002). Simultaneous laser raman-rayleigh-lif measurements and numerical modeling results of a lifted turbulent H₂/N₂ jet flame in a vitiated coflow. *Proceedings in the combustion institute*, 20:1881–1888.
- [Chen and Axelbaum, 2005] Chen, R. and Axelbaum, R. L. (2005). Scalar dissipation rate at extinction and the effects of oxygen-enriched combustion. *Combustion and Flame*, 142:62–71.
- [Cheng et al., 1992] Cheng, T. S., Wehrmeyer, J. A., and Pitz, R. W. (1992). Simultaneous temperature and multispecies measurement an a lifted hydrogen diffusion flame. *Combustion and Flame*, 91:323–345.
- [Chiesa et al., 2005] Chiesa, P., Lozza, G., and Mazzocchi, L. (2005). Using hydrogen as a gas turbine fuel. *Journal of Engineering for Gas Turbines and Power*, 127:73–80.
- [Coleman and Steele, 1983] Coleman, H. W. and Steele, W. G. (1983). *Experimentation, Validation, and Uncertainty Analysis for Engineers*. Mc Graw Hill, 3rd edition.
- [Ertesvåg, 2000] Ertesvåg, I. S. (2000). *Turbulent strøyming og Forbrenning*. Tapir - akademisk forlag.
- [Heck et al., 2009] Heck, R. M., Farrauto, R. J., and Gulati, S. T. (2009). *Catalytic air pollution control comersial technology*. WILEY, 3rd edition.
- [IEA, 2008] IEA (2008). *Key World Energy Statistics*. OECD/IEA.

Bibliography

- [Jakobsen, 2008] Jakobsen, H. A. (2008). *Chemical Reactor Modeling*. Springer.
- [Lefebvre and Ballal, 2010] Lefebvre, A. H. and Ballal, D. R. (2010). *Gas Turbine Combustion, Alternative Fuels and Emissions*. CRC Press, Taylor and Francis Group, 3rd edition.
- [Markides and Mastorakos, 2005] Markides, C. N. and Mastorakos, E. (2005). An experimental study of hydrogen autoignition in a turbulent co-flow of heated air. *Proceedings of the Combustion Institute*, 30:883–891.
- [MATLAB, 2010] MATLAB (2010). *version 7.11.0.584 (R2010b)*. The MathWorks Inc., Natick, Massachusetts.
- [MediaCollege, 2011] MediaCollege (2011). *Microphone Frequency Response*. <http://www.mediacollege.com/audio/microphones/frequency-response.html>.
- [Montgomery et al., 1998] Montgomery, C. J., Kaplan, C. R., and Oran, E. S. (1998). The effect of coflow velocity on a lifted methane-air jet diffusion flame. *Twenty-Seventh Symposium (International) on Combustion/The Combustion Institute*, pages 1175–1182.
- [North, 2010] North, A. (2010). Design of a vitiated coflow burner for elevated pressure experiments. Master’s thesis, University of California, Berkeley.
- [North et al., 2011] North, A. J., Dibble, R. W., Chen, J. Y., Federick, D. J., and Gruber, A. (2011). Liftoff heights of lifted N₂-in-H₂ jet flames issuing into a vitiated co-flow measured using schlieren imaging. *7th US National Technical Meeting of the Combustion Institute*.
- [Pello, 2008] Pello, C. (2008). Fundamentals of combustion processes. Reading Materials for ME 140 University of California, Berkeley.
- [Pitt, 1989] Pitt, W. M. (1989). Importance of isothermal mixing process to the understanding of lift-off and blowout of turbulent jet diffusion flames. *Combustion and Flame*, 76:197–212.
- [Pope, 2000] Pope, S. B. (2000). *Turbulent Flows*. Cambridge University Press.
- [Smith, 1997] Smith, S. W. (1997). *The Scientist and Engineer’s Guide to Digital Signal Processing*. California Technical Publishing.

- [Ströhle and Myhrvold, 2007] Ströhle, J. and Myhrvold, T. (2007). An evaluation of detailed reaction mechanisms for hydrogen combustion under gas turbine conditions. *International Journal of Hydrogen Energy*, 32:125–135.
- [Su, 1998] Su, L. K. (1998). Measurements of the three-dimensional scalar dissipation rate in gas-phase planar turbulent jets. *Center for Turbulence Research Annual Research Briefs 1998*, pages 35–46.
- [Tacke et al., 1998] Tacke, M. M., Geyer, D., Hassel, E. P., and Janicka, J. (1998). A detailed investigation of the stabilization point of lifted turbulent diffusion flames. *Twenty-Seventh Symposium (International) on Combustion/The Combustion Institute*, pages 1157–1165.
- [Toong, 1983] Toong, T.-Y. (1983). *The Dynamics of Reacting Fluids*. Mc Graw Hill.
- [Turns, 2006] Turns, S. R. (2006). *An Introduction to Combustion*. Mc Graw Hill, 2nd edition.
- [Verhelst and Walner, 2009] Verhelst, S. and Walner, T. (2009). Hydrogen-fueled internal combustion engines. *Progress in Energy and Combustion*, 35:490–527.
- [Vervisch and Poinso, 1998] Vervisch, L. and Poinso, T. (1998). Direct numerical simulation of non-premixed turbulent flames. *Annual Review of Fluid Mechanics*, 30:655–691.
- [Warnatz et al., 2001] Warnatz, J., Maas, U., and Dibble, R. W. (2001). *Combustion*. Springer, Berlin, 3rd edition.
- [Wheeler and Ganji, 2004] Wheeler, A. J. and Ganji, A. R. (2004). *Introduction to Engineering Experimentation*. Prentice Hall, 3rd edition.
- [White et al., 2006] White, C. M., Steeper, R. R., and Lutz, A. E. (2006). The hydrogen-fueled internal combustion engine: a technical review. *International Journal of Hydrogen Energy*, 31:1292–1305.
- [White, 2006] White, F. M. (2006). *Viscous Fluid Flow*. Mc Graw Hill, 3rd edition.
- [White, 2008] White, F. M. (2008). *Fluid Mechanics*. Mc Graw Hill, 6th edition.
- [Wu et al., 2009] Wu, Y., Lu, Y., Al-Rahbi, I. S., and Kalghatgi, G. T. (2009). Prediction of the liftoff, blowout and blowoff stability limits of

Bibliography

pure hydrogen/hydrocarbon mixture jet flames. *International Journal of Hydrogen Energy*, 34:5940–5945.

[Züttel et al., 2008] Züttel, A., Borgschulte, A., and Schlapbach, L. (2008). *Hydrogen as a future energy carrier*. WILEY VCH.

A. Table of results from the experiments

A.1. Results from Audio Recordings

The results from the audio recordings are shown in table A.2 to A.7 where f is the frequency.

Table A.1.: Audio results, $V_{jet}=300\text{m/s}$.

Φ_{cflow}	Y_{N_2}	f [Hz]
$\Phi = 0.20$	0.276	0.4
	0.290	3.3
	0.298	7.8
	0.310	16.1
	0.326	20.7
	0.340	23.0
	0.355	21.8
	0.370	15.5
	0.383	12.5
	0.397	9.3
	0.411	5.4
	0.432	2.3
	0.439	1.9
0.449	2.7	

A. Table of results from the experiments

Table A.2.: Audio results, $V_{jet}=300\text{m/s}$, continued.

Φ_{coflow}	Y_{N_2}	f [Hz]
$\Phi = 0.22$	0.342	0.6
	0.367	1.4
	0.393	2.2
	0.412	4.1
	0.429	6.7
	0.448	20.5
	0.461	23.7
	0.471	14.2
	0.484	4.3
	0.488	1.9
$\Phi = 0.24$	0.491	0.2
	0.448	0.1
	0.471	2.8
	0.487	23.0
	0.498	19.4
	0.502	0.7
	0.504	0.4
$\Phi = 0.25$	0.510	0
	0.477	0.4
	0.490	7.1
	0.499	26.5
	0.505	9.1
$\Phi = 0.27$	0.508	0.1
	0.510	0
	0.514	18.5
	0.518	1.0

A.1. Results from Audio Recordings

Table A.3.: Audio results, $V_{jet}=400\text{m/s}$.

Φ_{cflow}	Y_{N_2}	f [Hz]
$\Phi = 0.20$	0.218	0.4
	0.232	3.4
	0.254	15.0
	0.274	18.0
	0.304	20.8
	0.324	13.9
	0.349	11.3
	0.366	7.6
	0.388	4.3
	0.407	2.1
	0.425	0.6
	0.439	0.1
	$\Phi = 0.21$	0.221
0.244		3.8
0.257		6.0
0.277		10.5
0.293		12.9
0.313		13.8
0.330		15.5
0.347		7.7
0.365		6.0
0.374		5.8
0.385		5.7
0.401		1.8
0.413		0.8
0.424	0.6	
0.428	0.1	

A. Table of results from the experiments

Table A.4.: Audio results, $V_{jet}=400\text{m/s}$, continued.

Φ_{coflow}	Y_{N_2}	f [Hz]
$\Phi = 0.22$	0.276	0.8
	0.292	1.2
	0.310	2.0
	0.324	3.5
	0.336	4.7
	0.349	11.0
	0.358	13.0
	0.371	16.8
	0.384	19.0
	0.396	22.0
	0.411	25.0
	0.428	22.1
	0.444	16.5
	0.464	11.0
	0.476	7.0
0.487	0.4	
0.495	0.1	
$\Phi = 0.23$	0.393	0.5
	0.430	2.7
	0.455	6.5
	0.467	12.0
	0.478	27.0
	0.490	26.2
	0.500	14.2
	0.503	3.7
0.535	0	
$\Phi = 0.24$	0.451	0.6
	0.465	2.4
	0.477	4.6
	0.482	6.0
	0.496	22.0
	0.510	11.5
	0.517	0.9
0.521	0.1	

A.1. Results from Audio Recordings

Table A.5.: Audio results, $V_{jet}=400\text{m/s}$, continued.

Φ_{cflow}	Y_{N_2}	f [Hz]
$\Phi = 0.25$	0.434	0.3
	0.453	0.8
	0.471	2.6
	0.493	17.0
	0.505	21.0
	0.517	12.1
	0.524	0.3
$\Phi = 0.26$	0.483	0.8
	0.505	6.5
	0.517	21.0
	0.525	14.7
	0.530	1.6
	0.535	0
$\Phi = 0.27$	0.510	0
	0.523	10.0
	0.530	16.0
	0.534	13.0
	0.539	0

A. Table of results from the experiments

Table A.6.: Audio results, $V_{jet}=500\text{m/s}$.

Φ_{coflow}	Y_{N_2}	f [Hz]
$\Phi = 0.20$	0.180	3.1
	0.190	3.4
	0.196	5.0
	0.204	6.3
	0.215	6.9
	0.229	7.9
	0.246	7.2
	0.264	3.4
	0.280	2.7
	0.293	2.2
	0.314	2.5
$\Phi = 0.22$	0.334	1.8
	0.351	1.6
	0.210	1.3
	0.229	2.8
	0.244	4.9
	0.261	8.5
	0.280	15.7
	0.294	22.1
	0.314	25.4
	0.342	20.2
	0.364	18.7
0.379	12.3	
0.393	8.5	
0.411	4.6	
0.431	0.8	
$\Phi = 0.24$	0.360	2.0
	0.396	5.2
	0.423	10.0
	0.446	17.4
	0.464	21.0
	0.496	26.0
	0.512	23.0
	0.528	10.6
0.535	1.7	
0.542	0.1	

A.2. Results from High Speed Videos

Table A.7.: Audio results, $V_{jet}=500\text{m/s}$, continued.

Φ_{cflow}	Y_{N_2}	f [Hz]
$\Phi = 0.25$	0.421	0.5
	0.446	3.7
	0.486	22.0
	0.505	25.0
	0.532	10.5
	0.540	2.3
	0.545	0.1
$\Phi = 0.27$	0.550	10.0
	0.562	16.0
	0.566	2.0

A.2. Results from High Speed Videos

The results from the high speed videos can be seen in table A.8 to A.11 where f is the frequency.

Table A.8.: Video results, $V_{jet}=300\text{m/s}$.

Φ_{cflow}	Y_{N_2}	f [Hz]
$\Phi = 0.20$	0.289	1.9
	0.301	3.0
	0.319	0.3
	0.322	11.6
	0.337	19.3
	0.352	19.5
	0.372	18.6
	0.394	13.7
	0.412	10.3
	0.427	6.2
	0.430	4.5
	0.452	1.0

A. Table of results from the experiments

Table A.9.: Video results, $V_{jet}=400\text{m/s}$.

Φ_{coflow}	Y_{N_2}	f [Hz]
$\Phi = 0.20$	0.218	1.7
	0.232	3.6
	0.254	9.2
	0.274	13.5
	0.304	18.0
	0.324	14.6
	0.349	10.5
	0.366	8.4
	0.388	2.9
	0.407	1.2
	0.425	0.5
	0.439	0.1
	$\Phi = 0.21$	0.229
0.244		4.0
0.257		6.9
0.277		11.6
0.293		13.4
0.313		14.4
0.330		16.0
0.347		8.5
0.365		5.9
0.374		5.2
0.385		2.3
0.401		0.5
0.413		0.9
0.424	0	
0.428	0	

A.2. Results from High Speed Videos

Table A.10.: Video results, $V_{jet}=400\text{m/s}$, continued.

Φ_{coflow}	Y_{N_2}	f [Hz]
	0.258	0.5
	0.272	1.0
	0.302	3.0
	0.322	3.2
	0.349	12.4
	0.364	16.9
$\Phi = 0.22$	0.391	23.6
	0.412	27.2
	0.434	19.0
	0.455	8.7
	0.468	2.6
	0.473	1.3
	0.493	0.3

A. Table of results from the experiments

Table A.11.: Video results, $V_{jet}=500\text{m/s}$.

Φ_{coflow}	Y_{N_2}	f [Hz]
$\Phi = 0.20$	0.180	0.3
	0.190	2.8
	0.196	5.4
	0.204	7.3
	0.215	7.3
	0.229	7.5
	0.246	5.8
	0.264	3.4
	0.280	3.1
	0.293	3.0
	0.314	3.2
	0.334	1.4
	0.351	1.0
$\Phi = 0.22$	0.210	2.7
	0.229	2.7
	0.244	4.8
	0.261	6.8
	0.280	11.2
	0.294	17.5
	0.314	22.8
	0.342	22.0
	0.364	17.6
	0.379	11.8
	0.393	6.8
0.411	2.0	
0.413	0.4	

B. Calculation of the systematic uncertainty

Accuracy of the pressure transducers for the jet H₂ and air flow: 150 psig max, accuracy 1% of maximum. This leads to a maximum uncertainty of $u_{max}= 1.5$ psig.

Accuracy of the pressure transducers for the nitrogen and co-flow hydrogen: 300 psi max, accuracy 0.4% of maximum. This leads to a maximum uncertainty of $u_{max}=1.2$ psig.

The uncertainties in the pressure transducers results in uncertainties in the four different flow measurements according to the following equation:

$$w_x = \frac{u_{max_x}}{P_x} \quad (\text{B.1})$$

The systematic uncertainty is calculated for two data points with $V_{jet}=400$ m/s, $\Phi_{cf}=0.22$ and $Y_{N_2}=0.371$ and 0.464 .

The equation for the uncertainty in the results caused by uncertainties in the pressure transducers is as follows:

$$w_{pt} = \left[\left(\frac{df}{dY_{N_2}} \cdot w_{N_2} \right)^2 + \left(\frac{df}{d\Phi_{cf}} \cdot w_{H_2,cf} \right)^2 + \left(\frac{df}{d\Phi_{cf}} \cdot w_{air,cf} \right)^2 + \left(\frac{df}{dV_{jet}} \cdot w_{H_2,jet} \right)^2 \right]^{1/2} \quad (\text{B.2})$$

where w_{N_2} is the uncertainty related to the pressure transducer for the nitrogen jet flow, $w_{H_2,cf}$ is the uncertainty related to the pressure transducer for the hydrogen co-flow, $w_{air,cf}$ is the uncertainty related to the pressure transducer for the air co-flow and $w_{H_2,jet}$ is the uncertainty related to the pressure transducer for the hydrogen jet flow.

Here the co-flow has two terms, one with air and one with hydrogen. The jet velocity has only one term, the hydrogen jet term. It is assumed that the

B. Calculation of the systematic uncertainty

term that calculates the uncertainty in the nitrogen dilution mole fraction takes care of the uncertainty related to N_2 and the velocity term takes care of the uncertainty in the hydrogen jet flow.

The calibration of the orifices was performed over periods of two minutes. It is assumed that the error in the two minutes might be 1 second. this leads to an uncertainty of $w_{cal} = \frac{1}{120}$. The equation for the uncertainty in the results caused by calibration errors is as follows:

$$w_{cal} = \left[\left(\frac{df}{dY_{N_2}} \cdot w_{cal} \right)^2 + \left(\frac{df}{d\Phi_{cf}} \cdot w_{cal} \right)^2 + \left(\frac{df}{d\Phi_{cf}} \cdot w_{cal} \right)^2 + \left(\frac{df}{dV_{jet}} \cdot w_{cal} \right)^2 \right]^{1/2} \quad (B.3)$$

The total systematic uncertainty is:

$$w_R = \sqrt{w_{pt}^2 + w_{cal}^2} \quad (B.4)$$

Table B.1 lists up the values for the two cases.

Table B.1.: Calculation of systematic uncertainty for a flame with $V_{jet}=400$ m/s and $\Phi_{co-flow}=0.22$

variable	$Y_{N_2} = 0.371$	$Y_{N_2} = 0.464$
P_{N_2} [psig]	41	55
$P_{H_2,jet}$ [psig]	19	15
$P_{H_2,cf}$ [psig]	25	25
$P_{air,cf}$ [psig]	60	60
$\frac{df}{dY_{N_2}}$	2.32	-2.96
$\frac{df}{d\Phi_{cf}}$	111.4	3.0
$\frac{df}{dV_{jet}}$	-0.006	0.102
w_{N_2}	0.0293	0.0218
$w_{H_2,cf}$	0.048	0.048
$w_{air,cf}$	0.025	0.025
$w_{H_2,jet}$	0.079	0.100
w_{pt}	6.03	0.18
w_{cal}	1.31	0.04
w_R	6.17	0.18

C. Calculation of random uncertainty

The random counting uncertainty and time step uncertainty was found for the cases of $V_{jet} = 400$ m/s, $\Phi_{co-flow} = 0.22$ and $Y_{N_2} = 0.361$ and $Y_{N_2} = 0.464$. The methods used were the same as the methods used in chapter 7.5. The results for the random counting uncertainty can be seen in table C.1.

Table C.1.: Calculation of random counting uncertainty for $V_{jet} = 400$ m/s and $\Phi = 0.22$.

N_2 Dilution, Y_{N_2}	\bar{f} [Hz]	S_x	$\pm P_{\bar{x}}$	$\pm P_{\bar{x}}$ %
0.361	16.9	0.54	0.67	4.0
0.464	11.5	0.61	0.75	6.5

The time step uncertainty for a time step of 40 s can be seen in table C.2.

Table C.2.: Calculation of time step uncertainty for $V_{jet} = 400$ m/s and $\Phi = 0.22$ with $t = 40$ s.

N_2 Dilution, Y_{N_2}	\bar{f} [Hz]	S_x	$\pm P_{\bar{x}}$	$\pm P_{\bar{x}}$ %
0.361	17.3	0.11	0.13	1.7
0.464	10.0	0.18	0.22	5.0

D. MATLAB scripts

Here the MATLAB scripts used in the signal analysis are given.

D.1. Count peaks script

This is the script used in the method of counting peaks:

```
clear
clc
close all
[background, Fs1, nbits1] = wavread('lifted_flame');
[sound_bite, Fs, Nbits] = wavread('phi0222.N243.14');
                                % Reads the sound file

n=1;
L=882000*n;
sound_bite=sound_bite((882000*(n-1))+1:L);
%(Fs is the sampling frequency, 44100 Hz)
background=background(1:44100);
N = length(sound_bite);
seklength = round(N/Fs);           % How many seconds is the sound file
t = linspace(0, round(N*1/Fs), N); % time vector

figure(1);
plot(t, sound_bite);

fw=30;                               % Filter width
for i=(1):(length(sound_bite)-fw)
sound_bite(i)=mean(abs(sound_bite(i:i+fw)));
end
ave=mean(sound_bite);
sound_bite=sound_bite-ave;

figure(2);
plot(t, sound_bite);
xlabel('Time, [s]')
ylabel('Normalized Amplitude')
```

D. MATLAB scripts

```
%axis ([0 1 -0.4 0.4])
title('Filtered Time - Amplitude Response For Jet Flame')

[pks_1, locs_1] = findpeaks(sound_bite, 'minpeakdistance',
441, 'minpeakheight', 0.54); % Finds peaks.
    % The last number sets minimum peak value
    %Look at figure 1 to see where to put the line

figure(3);
SUBPLOT(2,1,1), plot(locs_1, pks_1+1, 'k^', 'markerfacecolor', [1 0 0])
SUBPLOT(2,1,2), plot(t, sound_bite)

Number_of_peaks_filtered = length(pks_1)
Number_of_peaks_filtered_per_sekund =
Number_of_peaks_filtered/seklength
```

D.2. FFT script

The MATLAB code used in the FFT of the sound signal is as follows:

```
clear
clc
close all

[sound_bite, Fs, nbits] = wavread('phi020_N240-65.1.wav');

sound_bite=sound_bite(1:882000);
t1=linspace(0,length(sound_bite)/Fs,length(sound_bite));
%plot(t1(1:400), sound_bite(1:400))

figure(1)
plot(t1(50000:100000), sound_bite(50000:100000))
xlabel('Time, [s]')
ylabel('Normalized Amplitude')
title('Unfiltered Time - Amplitude Response For Jet Flame')

N=length(sound_bite);
f = Fs/N .* (0:N-1);
freq=fft(sound_bite,N); % Function that returns the
freq_norm = abs(freq(1:N)) ./ (N/2); % discrete fourier transform
```

```

% of a vector
figure(2)
plot(f(1:500),freq_norm(1:500));
xlabel('Frequency, [Hz]')
ylabel('Amplitude')
title('Frequency Response For Jet Flame')

```

D.3. Integral method

The code for the integral method is as follows:

```

clear
clc
close all

[sound_bite, Fs, nbits] = wavread('phi020_N240_65_1.wav');
L=200000;
Lp=200000;
%sound_bite=sound_bite(1:L);
t1=linspace(0,length(sound_bite)/Fs,length(sound_bite));

figure(1);
plot(t1(1:Lp), sound_bite(1:Lp))
plot(t1, sound_bite);
xlabel('time (s)')
ylabel('Amplitude')
title('Unfiltered Time - Amplitude Response For Jet Flame')

N=length(sound_bite);
f = Fs/N .* (0:N-1);
freq=fft(sound_bite,N); % FFT of the signal
freq_norm = abs(freq(1:N)) ./ (N/2);

integration_end=20; % sets the integration limits,
i_int_end=round(N*integration_end/Fs)% from zero to integration_end
% while freq_norm(i)>1E-6
% i=i+1;
% end
int=trapz(freq_norm(2:i_int_end));
j=2;
int2=0;
while int2<int/2
    int2=trapz(freq_norm(2:j));

```

D. MATLAB scripts

```
        j=j+1;
end
freq_half=f(j)           % Prints the frequency that divides the
                        % area in two

fq_max=20;
nf_max=round(N*fq_max/Fs);

figure(2)
plot(f(1:nf_max),freq_norm(1:nf_max));% plots the FFT from 1 to a
xlabel('Frequency, [Hz]')           %chosen maximum value, fq_max
ylabel('Amplitude')
title('Filtered Frequency - Amplitude Response For Jet Flame')
```

D.4. Background correction

The code including background correction is as follows:

```
clear
clc
close all

[background, Fs1, nbits1] =wavread('noflame.wav');% recording of
                                                %background noise

[sound.bite, Fs, nbits] = wavread('phi020.N223_20.wav');
L=200000;
Lp=200000;
background=background(1:L);
sound.bite=sound.bite(1:L);
t1=linspace(0,length(sound.bite)/Fs,length(sound.bite));

figure(1)
plot(t1(1:Lp),sound.bite(1:Lp))
xlabel('Time, [s]')
ylabel('Normalized Amplitude')
title('Unfiltered Time - Amplitude Response For Jet Flame')

fw=200;
modulator=5;
for i=(1):(length(sound.bite)-fw)
    if mod(i,modulator)==0
        sound.bitef(i/modulator)=mean(abs(sound.bite(i:i+fw)));
    end
end
```

```

sound_bitef=sound_bitef(1:round(Lp/modulator)-fw);
fNorm = 400 / (Fs/2);
[b,a] = butter(10, fNorm, 'low');
sound_bitef = filtfilt(b, a, sound_bite);
figure
freqz(sound_bitef)
t2=linspace(0,length(sound_bitef)/Fs*modulator,length(sound_bitef));

figure(2)
plot(t2(1:(round(Lp/modulator)-fw)),sound_bitef
(1:(round(Lp/modulator)-fw)))
xlabel('Time, [s]')
ylabel('Normalized Amplitude')
title('Filtered Time - Amplitude Response For Jet Flame')

N1=length(background);
f1 = Fs/N1 .* (0:N1-1);
freq1=fft(background,N1);
freq_norm_background = abs(freq1(1:N1)) ./ (N1/2);

N=length(sound_bite);
f = Fs/N .* (0:N-1);
freq=fft(sound_bite,N);
freq_norm1= abs(freq(1:N)) ./ (N/2);
freq_norm = freq_norm1-freq_norm_background;
freq_norm(freq_norm==0) = eps;
freq_norm = 20 * log10(freq_norm);
i=1

integration_end=15;
i_int_end=round(N*integration_end/Fs)
% while freq_norm(i)>1E-6
%     i=i+1;
% end
int=trapz(freq_norm(1:i_int_end));
j=1;
int2=0;
while int2<=int/2
    int2=trapz(freq_norm(1:j));
    j=j+1;
end
freq_half=f(j)
fq_max=15;
nf_max=round(N*fq_max/Fs);

figure(3)
plot(f(1:nf_max),freq_norm1(1:nf_max));
xlabel('Frequency (Hz)')
ylabel('Amplitude')

```

D. MATLAB scripts

```
title('Raw Unfiltered Frequency-Amplitude Response For Jet Flame')

figure(4)
amp_max=max(freq_norm(1:nf_max))*1.1;
plot(f(1:nf_max),freq_norm(1:nf_max));
axis([0 fq_max 0 amp_max]);
xlabel('Frequency (Hz)')
ylabel('Amplitude')
title('Background Corrected Unfiltered Frequency -
Amplitude Response For Jet Flame')

fw2=20;

for i=(1):(length(freq_norm)-fw2)
    freq_normf(i+round(fw2/2))=mean(freq_norm(i:i+fw2));
end

figure(5)
amp_max=max(freq_normf(1:nf_max))*1.1;
plot(f(1+round(fw2/2):nf_max),freq_normf(1+round(fw2/2):nf_max));
axis([0 fq_max 0 amp_max]);
xlabel('Frequency (Hz)')
ylabel('Amplitude')
title('Background Corrected Filtered Frequency -
Amplitude Response For Jet Flame')
```